

Lifetime of the Outer Solar System Nebula From Carbonaceous Chondrites

Cauê S. Borlina^{1,2} , Benjamin P. Weiss¹ , James F. J. Bryson³, and Philip J. Armitage^{4,5} 

¹Department of Earth, Atmospheric and Planetary Sciences, Massachusetts Institute of Technology, Cambridge, MA, USA,

²Department of Earth and Planetary Sciences, Johns Hopkins University, Baltimore, MD, USA, ³Department of Earth Sciences, Oxford University, Oxford, UK, ⁴Center for Computational Astrophysics, Flatiron Institute, New York, NY, USA,

⁵Department of Physics and Astronomy, Stony Brook University, Stony Brook, NY, USA

Key Points:

- Paleomagnetic measurements of CO chondrites suggest solar nebula dissipation within 2.7–5.1 Myr after the formation of the solar system
- The solar nebula went through a two-timescale evolution, consistent with dissipation through photoevaporation and/or magnetized winds
- We discuss the uncertainties associated with paleomagnetic measurements of bulk chondrites and recommend future directions for the field

Supporting Information:

Supporting Information may be found in the online version of this article.

Correspondence to:

C. S. Borlina,
csciase1@jhu.edu

Citation:

Borlina, C. S., Weiss, B. P., Bryson, J. F. J., & Armitage, P. J. (2022). Lifetime of the outer solar system nebula from carbonaceous chondrites. *Journal of Geophysical Research: Planets*, 127, e2021JE007139. <https://doi.org/10.1029/2021JE007139>

Received 20 NOV 2021

Accepted 23 MAY 2022

Author Contributions:

Conceptualization: Cauê S. Borlina, Benjamin P. Weiss

Data curation: Cauê S. Borlina

Formal analysis: Cauê S. Borlina

Funding acquisition: Benjamin P. Weiss

Investigation: Cauê S. Borlina, Benjamin P. Weiss

Methodology: Cauê S. Borlina, Benjamin P. Weiss

Project Administration: Benjamin P. Weiss

Software: Cauê S. Borlina

Abstract The evolution and lifetime of protoplanetary disks (PPDs) play a central role in the formation and architecture of planetary systems. Astronomical observations suggest that PPDs evolve in two timescales, accreting onto the star for up to several million years (Myr) followed by gas dissipation within $\lesssim 1$ Myr. Because solar nebula magnetic fields are sustained by the gas of the protoplanetary disk, we can use paleomagnetic measurements to infer the lifetime of the solar nebula. Here, we use paleomagnetic measurements of meteorites to constrain this lifetime and investigate whether the solar nebula had a two-timescale evolution. We report on paleomagnetic measurements of bulk subsamples of two CO carbonaceous chondrites: Allan Hills A77307 and Dominion Range 08006. If magnetite in these meteorites can acquire a crystallization remanent magnetization that recorded the ambient field during aqueous alteration, our measurements suggest that the local magnetic field strength at the CO parent body location was $<0.9 \mu\text{T}$ at some time between 2.7 and 5.1 Myr after the formation of calcium-aluminum-rich inclusions. Coupled with previous paleomagnetic studies, we conclude that the dissipation of the solar nebula in the 3–7 AU region occurred <1.5 Myr after the dissipation of the nebula in the 1–3 AU region, suggesting that protoplanetary disks go through a two-timescale evolution in their lifetime, consistent with dissipation by photoevaporation and/or magnetohydrodynamic winds. We also discuss future directions necessary to obtain robust records of solar nebula fields using bulk chondrites, including obtaining ages from meteorites and experimental work to determine how magnetite acquires magnetization during chondrite parent body alteration.

Plain Language Summary Magnetic fields play an important role during planetary formation. That is because during the first few million years of the solar system, when only gas and dust were present, magnetic fields are coupled to the gas. Meteorites, rocks that formed during the early stages of the solar system that made their way to the Earth, could have recorded this ambient magnetic field and maintained this record for billions of years. By conducting paleomagnetic measurements of meteorites and coupling our measurements with previous work, we establish when the gas in the early solar system dissipated. Our results indicate that the gas existed for ~ 3 million years and dispersed within <1.5 million years. This is consistent with mechanisms for gas dispersal that involve heating from the young Sun and magnetic-driven winds expelling gas from the solar system. We also discuss uncertainties associated with paleomagnetic measurements and what the community can do in the future to obtain robust records of magnetic fields from the early solar system.

1. Introduction

The lifetimes of protoplanetary disks (PPDs) have important implications for the formation of planetary systems that emerge from them. Determining the lifetime of PPDs (i.e., the dissipation of the gas) constrains the formation time of gas giants and when gas-driven planetary migration can occur. The lifetimes of PPDs have been measured astronomically through observations of dust infrared spectral energy distributions (SEDs) (Haisch et al., 2001; Hernández et al., 2007). SED observations have provided evidence that disks pass through different stages during their evolution from that of protostars to transition disks (disks that have low or no near-infrared excess and high mid-to far-infrared excess) and to debris disks (no remaining gas) (Ercolano & Pascucci, 2017; Owen, 2016). With the exception of a few observed PPDs that are likely in the transition phase, the majority ($\sim 90\%$) of observed PPDs are either in the PPD phase with a protostar or completely dissipated (Owen, 2016). This observation has been interpreted to suggest that PPDs have a two time-scale evolution during their lifetime: during

© 2022 The Authors.

This is an open access article under the terms of the [Creative Commons Attribution-NonCommercial License](#), which permits use, distribution and reproduction in any medium, provided the original work is properly cited and is not used for commercial purposes.

Supervision: Benjamin P. Weiss
Visualization: Cauê S. Borlina
Writing – original draft: Cauê S. Borlina
Writing – review & editing: Cauê S. Borlina, Benjamin P. Weiss, James F. J. Bryson, Philip J. Armitage

the first evolutionary stage, which lasts $\sim 3\text{--}5$ million years (Myr), the disk evolves via magnetohydrodynamic and/or hydrodynamic processes, with angular momentum transported outward that enables accretion onto the star (Armitage & Kley, 2019; Gorti et al., 2016); during the second stage, the remaining gas disperses rapidly, in $\lesssim 1$ Myr (Ercolano & Pascucci, 2017). Several modes of disk dispersal have been proposed (Ercolano & Pascucci, 2017), including photoevaporation by the central star (Alexander et al., 2006) or a nearby high-mass star (Concha-Ramírez et al., 2019; Scally & Clarke, 2001), magnetohydrodynamic (MHD) winds (Armitage et al., 2013; Bai, 2016; Shadmehri & Ghoreyshi, 2019; Suzuki et al., 2016), planet formation (Zhu et al., 2011), grain growth (Dullemond & Dominik, 2005), and close-binary effects (Ireland & Kraus, 2008). The two-timescale evolution is generally consistent with gas dissipation by photoevaporation and/or magnetohydrodynamic winds. Because the lifetimes of PPDs are far greater than the times over which we can observe them, testing the two-timescale hypothesis through observations of any one PPD is essentially impossible.

However, the two-timescale hypothesis can be tested using paleomagnetic measurements of our solar system's PPD, also known as the solar nebula. Due to the coupling of magnetic fields with gas, the nebular magnetic field is a proxy for the presence of gas in the disk, and thus the lifetime of the disk (Wang et al., 2017; Weiss et al., 2021). By obtaining paleomagnetic measurements from meteorites that formed at different times and locations, it is possible to constrain the lifetime and spatial evolution of the PPD of our solar system. Previous paleomagnetic studies of meteorites have provided evidence for a large-scale magnetic field present in the disk up to at least $3.9^{+0.4}_{-0.5}$ Myr after the formation of the calcium-aluminum-rich inclusions (CAIs) (Borlina et al., 2021; Cournede et al., 2015; Fu et al., 2014). Additional studies have also found evidence for the dissipation of the gas at <3 AU (inner solar system) by 3.2–5.0 Myr after CAI-formation, with Pb-Pb ages indicating a mean dissipation time by 3.71 ± 0.2 Myr after CAI-formation (Wang et al., 2017; Weiss et al., 2021).

Here we use carbonaceous chondrites to obtain better constraints on the timescale of the dissipation of the solar nebula. Carbonaceous chondrites are unmelted accretional aggregates of refractory inclusions (CAIs and ameboid olivine aggregates), chondrules, and matrix, which likely formed in the 3–7 AU region (i.e., outer solar system) (Scott & Krot, 2013). In this study, we investigate the magnetic record of bulk subsamples of carbonaceous chondrites that contain all of these constituents. If not overprinted or remagnetized, chondrules and refractory inclusions are expected to carry pre-accretional magnetic records, while the matrix would have recorded a post-accretional magnetic record obtained during parent body alteration. Paleomagnetic measurements conducted with bulk samples are likely to provide magnetic records from the matrix material, because if chondrules and refractory inclusions are randomly oriented in the bulk and, even if magnetized, the magnetic moments of the inclusions cancel out, the matrix would dominate the magnetic record (see Supplementary Information).

We report on paleomagnetic measurements of bulk matrix-rich material of two carbonaceous chondrites from the CO group. A previous study of the CV chondrite Kaba provided an upper limit on the magnetic field at 3–7 AU of <0.3 μT at $4.2^{+0.8}_{-0.7}$ Myr after CAI-formation (Doyle et al., 2014; Gattacceca et al., 2016). We further investigate this region by targeting another group of carbonaceous chondrites that likely acquired a post-accretional magnetic record in this region but that, unlike Kaba, is much less likely to carry thermally induced parent body magnetic overprints. If magnetite could have acquired its magnetic record during alteration in the parent body, we show that the matrices of the CO chondrites carry no stable natural remanent magnetization (NRM) despite having high fidelity magnetic recording properties and ferromagnetic minerals that formed after accretion. We show that the lack of magnetization in the matrix of the CO chondrites, together with previous paleomagnetic measurements, suggests that the dissipation of the outer solar system nebula occurred by ~ 4.2 Myr after CAI-formation. By comparing the inner and outer solar system lifetimes of the nebula, we find that the outer solar nebula dissipated <1.5 Myr after the dissipation of the inner solar nebula, suggesting that our solar nebula passed through a dual-timescale evolution. We also discuss future work necessary to obtain robust records of the solar nebula by conducting paleomagnetic and rock magnetic measurements of bulk chondrites. This includes obtaining more high-precision ages from relevant meteorites and conducting experimental work to establish the mechanisms for acquisition of magnetic field records during parent body alteration, including if secondary magnetite can record crystallization remanent magnetization (CRM) imparted by the solar nebula field.

2. Materials and Methods

2.1. Samples

In this study, we focused on the type 3.03 CO chondrite Allan Hills (ALH) A77307 (Bonal et al., 2007) and on the type 3.00 CO chondrite Dominion Range (DOM) 08006 (Davidson et al., 2019). We selected these samples for several reasons. First, they formed magnetite during aqueous alteration on their parent body, so they can potentially provide constraints on the intensity of the local ambient magnetic field present during this process (Doyle et al., 2014). Second, they have ferromagnetic inclusions (e.g., magnetite; see below) with high-fidelity paleomagnetic properties (Alexander et al., 2018; Davidson et al., 2019; Sridhar et al., 2021). Third, they experienced very minor heating after parent body aqueous alteration, thereby better preserving a magnetic record dating to the time of this early alteration rather than slightly later during subsequent metamorphic heating and cooling (Davidson et al., 2019).

2.1.1. CO Carbonaceous Chondrites

Subsamples ALHA77307,157 (0.57 g) and DOM 08006,102 (2.8 g) were obtained from the US Antarctic Meteorite program (ANSMET). These were chipped from the meteorite at NASA Johnson Space Center (JSC) and did not contain any faces from band sawing at JSC that could have resulted in thermal remagnetization during cutting (e.g., Mighani et al. (2020); Tikoo et al. (2017)). Each subsample contained fusion crust on one of their faces.

Both meteorites experienced aqueous alteration and metamorphism on their parent body as indicated by the presence of a small fraction of metal (~ 2 vol.%) in the matrix and on the edges of chondrules, with most of the metal having been altered to magnetite (Bonal et al., 2016; Davidson et al., 2019). ALHA77307 experienced minor terrestrial weathering (Ae grade) and is estimated to have experienced a peak parent body metamorphic temperature between 200 and 300°C (Bonal et al., 2016). DOM 08006 has experienced minor terrestrial weathering (A/B grade) (Davidson et al., 2019) and has experienced similar or slightly lower peak temperatures in the parent body than ALHA77307 (Alexander et al., 2018). ALHA77307 and DOM 08006 did not exceed peak shock pressures of 5 GPa (Li et al., 2021; Scott et al., 1992). Overall, these observations suggest that ALHA77307 and DOM 08006 potentially carry records of magnetic fields acquired during parent body aqueous alteration.

The paleomagnetism of the CO chondrites has been briefly studied before (see Weiss et al. (2010) for the complete list of magnetic measurements with CO chondrites). A previous study conducted thermal demagnetization of saturation magnetization of four CO3 chondrites (Herndon et al., 1976), which found that one contains magnetite as the major magnetic phase, while the remaining samples contained magnetite along with iron metal as the main magnetic phases. Two previous exploratory paleomagnetic studies obtained paleointensities from CO chondrites. Measurements of bulk subsamples of the CO3 chondrite Acfer 333 identified a low coercivity component (0–15 mT) associated with an isothermal remanent magnetization (IRM) (likely from a collector's hand magnet) and a high coercivity component (30–120 mT) with a paleointensity of 6 μ T (Gattacceca & Rochette, 2004). Another study of bulk subsamples of the CO3.05 Yamato 81020 meteorite reported a high blocking temperature (320–640°C) component with a paleointensity of 9 μ T (Nagata et al., 1991). A paleomagnetic study of dusty olivine chondrules from ALHA77307 and DOM 08006 suggest that these meteorites have not been remagnetized since accretion to the parent body due to their random high coercivity magnetic directions among mutually oriented chondrules (Borlina et al., 2021). Here we use ALHA77307 and DOM 08006 to conduct a detailed paleomagnetic study with their bulk samples.

Previous mineralogical and petrological studies of the matrix of DOM 08006 have reported the presence of the ferromagnetic minerals kamacite ($\text{Fe}_x\text{Ni}_{1-x}$; with $x = 92\text{--}93$), magnetite, and pyrrhotite (Fe_{1-x}S ; with $x \sim 0$) (Alexander et al., 2018; Davidson et al., 2019; Schrader et al., 2021). Similar minerals have been reported for ALHA77307 (Alexander et al., 2018; Davidson et al., 2019; Grossman & Brearley, 2005; Schrader et al., 2021). The amount of magnetite (6–8 wt.%) is higher than sulfide (2–3 wt.%) and metals (1–2 wt.%) in the matrix of DOM 08006 (Alexander et al., 2018). Below we discuss why magnetite is likely to dominate the magnetic record of these samples. In a recent study, first-order reversal curves of DOM 08006 show a tri-lobate geometry, which is consistent with the magnetic carriers being predominately in vortex state (Sridhar et al., 2021). Because magnetite is the most abundant magnetic recorder and has the highest susceptibility (see Section 2.1.2), we conclude that the magnetite grains are dominantly in the vortex state, such that they are robust magnetic recorders with relaxation times greater than the age of the solar system (Nagy et al., 2019).

Because magnetite formed during parent body alteration (Davidson et al., 2019) and was not subsequently heated above 300°C, the magnetic record of these samples should be predominately in the form of CRM. No radiogenic ages have been reported for ALHA77307 and DOM 08006. Previous work determined a ^{53}Mn - ^{53}Cr age from aqueously formed fayalite of $5.1^{+0.5}_{-0.4}$ (2 σ) Myr after CAI-formation from MacAlpine Hills (MAC) 88107, a chondrite that formed from precursor material that had isotopic similarities to that of the CO parent body but has not been categorized as a CO chondrite (Doyle et al., 2014; Torrano et al., 2021). As such, this measured age is likely a proxy for the youngest possible age of magnetite formation on the CO chondrite parent body. Furthermore, Al-Mg ages of chondrules from CO chondrites suggest that they formed at 2.1 ± 0.8 Myr after CAI-formation (Borlina et al., 2021; Kita & Ushikubo, 2011) and recent modeling to explain the inventory of CAIs among different chondrite groups suggests that the CO chondrite parent body accreted at ~ 2.7 Myr after CAI-formation (Desch et al., 2018). Thus, we can place a lower limit on the alteration age of the CO chondrites of 2.7 Myr after CAI-formation, while an upper limit can be obtained by using MAC 88107's alteration age of 5.1 Myr after CAI-formation.

2.1.2. Magnetite as the Main Magnetic Carrier of Bulk Samples

Because bulk samples contain magnetic minerals that are pre-accretionary (e.g., kamacite) and post-accretionary (e.g., magnetite) in origin, it is important to establish which one of them will dominate the magnetization record. The NRM M , measured in the laboratory, is proportional to the magnetic field B , experienced by the sample, through:

$$M = \frac{\chi_R}{\mu_0} B, \quad (1)$$

where χ_R is the remanent susceptibility of the sample (Dunlop & Özdemir, 1997) and μ_0 is the vacuum permeability. We can write χ_R as (Kletetschka & Wiczeorek, 2017):

$$\chi_R \sim \frac{M_{rs}}{cM_s} = \frac{s}{c}, \quad (2)$$

where M_{rs} is the saturation remanent magnetization, M_s is the saturation magnetization, $s = M_{rs}/M_s$ is the squareness ratio, and c is a grain-shape dependent constant. Thus, for a sample that contains magnetite and kamacite, we can determine χ_R based on the sum of the remanent susceptibilities of each mineral through:

$$\chi_R = \chi_{\text{mag}} + \chi_{\text{kam}}, \quad (3)$$

$$\chi_{\text{mag}} \sim s_{\text{mag}}, \quad (4)$$

$$\chi_{\text{kam}} \sim s_{\text{kam}}, \quad (5)$$

where χ_{mag} and s_{mag} are the remanent susceptibility and squareness of the magnetite and χ_{kam} and s_{kam} are the remanent susceptibility and squareness of the kamacite, where we have assumed the grain-shape dependent constants for magnetite and kamacite are similar ($c_{\text{kam}} \sim c_{\text{mag}}$). Taking the ratio between Equations 4 and 5, we have:

$$\frac{\chi_{\text{mag}}}{\chi_{\text{kam}}} = \frac{s_{\text{mag}}}{s_{\text{kam}}}. \quad (6)$$

Because most magnetite is likely to be in the single-vortex and single-domain state while kamacite is likely to be multi-domain, we can assume $s_{\text{mag}}/s_{\text{kam}} > 100$ (Dunlop, 2002). Thus, $\chi_{\text{mag}} > 100\chi_{\text{kam}}$, indicating that magnetite will be the main magnetic carrier of the NRM in these samples.

2.1.3. Formation Region of the CO Carbonaceous Chondrites

The existence of a dichotomy in various stable isotopic systems (Kruijer et al., 2020; Scott et al., 2018) provides evidence that carbonaceous and non-carbonaceous meteorites formed in two distinct reservoirs. Although the exact locations for these reservoirs are unclear, it is generally thought that carbonaceous chondrites likely formed at >3 AU (Brasser & Mojzsis, 2020; DeMeo & Carry, 2014; Desch et al., 2018; Kruijer et al., 2020; Morbidelli et al., 2015). Measurements of water contents from CI, CM, CR, and LL chondrites provide evidence that carbonaceous chondrites formed at <7 AU (Sutton et al., 2017). Thus, we assume the formation region of the carbo-

naceous chondrites to be between 3 and 7 AU. We also assume that chondrite parent bodies originate from the midplane region of the PPD because drag forces on 0.1-mm-sized grains lead them to settle on the midplane of the PPD, resulting in the formation of the parent bodies in that region (Weiss et al., 2021).

2.2. Paleomagnetic and Rock Magnetic Experiments

Sample preparation and paleomagnetic analyses were conducted in the Massachusetts Institute of Technology (MIT) Paleomagnetism Laboratory. Samples from each meteorite were obtained by cutting with a wire saw cooled with ethanol to avoid acquisition of partial thermal remanent magnetization (pTRM) during cutting. We obtained eight mutually oriented samples from ALHA77307 and eleven mutually oriented samples from DOM 08006. Table 1 summarizes the mass and distance from the fusion crust to the outer edge of each sample. Paleomagnetic measurements were obtained in a magnetically shielded room (residual field ~ 200 nT) using a 2G Enterprises Superconducting Rock Magnetometer (SRM) 755R equipped with an automatic alternating field (AF) three-axis degausser and remagnetization system (Kirschvink et al., 2008). The three-axis moment noise level of the MIT 2G SRM is $<1 \times 10^{-12}$ Am² (Wang et al., 2017).

We AF demagnetized four samples from ALHA77307 (one containing fusion crust and the remaining from >1.8 mm away, into the interior) and eight samples from DOM 08006 (one containing fusion crust and the remaining from >1 mm away, into the interior). These samples were glued with cyanoacrylate cement onto a nonmagnetic quartz holder with magnetic moments of $<4 \times 10^{-12}$ Am². Samples were demagnetized with AF up to 145 mT to identify NRM components. We measured the magnetic moment after the AF application in each one of three directions and averaged the measurements to reduce spurious anhysteretic remanent magnetization (ARM) and gyroremanent magnetization (GRM) (Stephenson, 1993). We also applied ARMs (AC field of 260 mT and DC bias field of 50 μ T) to these samples and AF demagnetized them up to 145 mT. Paleointensities were estimated for these samples using the ARM method (Tikoo et al., 2014).

We followed the in-field zero-field zero-field in-field (IZZI) double heating protocol to obtain paleointensities (Yu et al., 2004). Heating measurements were performed using an ASC Scientific TD48-SC thermal demagnetizer in air with thermal accuracy better than $\pm 5^\circ\text{C}$. Samples were heated to the set temperature for 20 min and cooled within 40 min to room temperature. For ALHA77307 and DOM 08006, we initiated the IZZI protocol at 325 and 50 $^\circ\text{C}$, respectively, with steps below these being only thermally demagnetized (i.e., only heating in zero-field). The IZZI protocol was conducted in steps of 50 $^\circ\text{C}$, with a 50 μ T bias field and pTRM checks in 100 $^\circ\text{C}$ steps to determine whether thermochemical alteration could have occurred during the measurements. We note that failed pTRM checks in the absence of thermochemical alteration can also occur due to the presence of multi-domain magnetic carriers (Wang & Kent, 2021). Samples were taped to nonmagnetic quartz holders for measuring their magnetic moment. We thermally demagnetized four samples of ALHA77307 (two containing fusion crust and two interior samples) to identify NRM components and obtain additional paleointensity estimates. Initially, three interior samples of DOM 08006 were thermally demagnetized. However, two of these broke into two mutually oriented subsamples each at 350 $^\circ\text{C}$, leading to five thermally demagnetized samples. We conducted the IZZI protocol with two of these five samples. For three samples of ALHA (two fusion crusted and one interior), we removed low coercivity components (up to 21 mT) with AF demagnetization prior to the start of the IZZI protocol. We AF demagnetized to the same levels after each in-field step during the protocol. We also thermally demagnetized an ARM application (AC field of 145 mT and DC bias field of 50 μ T) of two ALHA77307 samples, following AF demagnetization of the NRM, to identify the Curie temperature of the ferromagnetic carriers.

Fits for both the ARM and IZZI paleointensities were obtained either using ordinary least squares (OLS) or reduced major axis (RMA) (Borlina et al., 2021; Smith, 2009). The quality of the results from the IZZI protocol were quantified using the PICRIT03 criteria (Paterson et al., 2014), which quantify thermochemical alteration during the protocol. Principal component analysis (PCA) was used to determine the direction and maximum angular deviation (MAD) of the magnetic components identified during the AF and thermal demagnetization (Kirschvink, 1980). To identify any origin trending components, we calculated the deviation angle (DANG). For samples in which DANG $<$ unanchored MAD, we calculated the PCA with an anchored fit (Tauxe & Staudigel, 2004).

Table 1
PCA Fits for ALHA77307 and DOM 08006

Sample	Weight (mg)	Distance from fusion crust (mm)	Component	Range (mT or °C)	<i>N</i>	Declination (°)	Inclination (°)	MAD (°)	DANG (°)	Anchored declination (°)	Anchored inclination (°)	Anchored MAD (°)	NRM/ARM
ALHA.a	5.51	fusion crusted	LC	0–20.5 mT	41	118.5	−4.9	4.6	—	—	—	—	4.8
			HC	26–410 mT	125	288.6	9.4	3.4	2.4	289.8	9.1	2.7	—
ALHA.b	7.68	1.8	LC	0–39 mT	64	148.1	11.5	1.1	2.5	149	12.1	1.5	2.1
			HC*	39–145 mT	87	175.5	3.7	33.7	—	—	—	—	—
ALHA.c	9.03	3.2	LC	0–58 mT	83	155.5	18.4	1.8	3.4	154.7	17.6	2.2	2.2
			HC*	58–145 mT	68	358	−1.3	40.9	—	—	—	—	—
ALHA.d	6.15	4.9	LC	0–55 mT	80	163.2	15.8	3.6	4.1	161.7	14.8	3.4	1
			HC*	55–145 mT	71	157.5	11.7	38.6	—	—	—	—	—
ALHA.e	1.10	fusion crusted	LC	0–18.5 mT	36	119.3	−20.3	3.9	—	—	—	—	—
			HT	251–580°C	17	277.4	0	10.9	19.2	290.7	0.7	10.7	—
ALHA.f	0.60	fusion crusted	LC	0–19 mT	39	123.7	−11	5.1	—	—	—	—	—
			HT	251–580°C	20	281.3	9.1	16.1	20.8	294.7	6.7	10.5	—
ALHA.g	2.00	4.5	LT	0–425°C	11	158.9	5.6	5.7	—	—	—	—	—
			HT*	425–580°C	12	357.1	−3.3	33.5	34.9	357.8	27.7	19.8	—
ALHA.h	0.60	5.8	LC	0–21 mT	42	152.8	6.5	5.5	—	—	—	—	—
			LT	51–375°C	8	112.9	−2.1	33.9	32.9	144.1	−4.5	14.1	—
			HT*	375–570°C	13	160.8	−6.6	30.5	—	—	—	—	—
DOM.a	1.03	fusion crusted	HC	0–145 mT	150	32.8	46.9	2.2	1.6	32.6	47.7	1.8	2.75
DOM.b	1.37	1.0	LC	0–10 mT	20	30.4	3.9	4	12.6	30.4	−4	6.6	0.14
			HC*	10–145 mT	131	147.7	−77.1	40.3	—	—	—	—	—
DOM.c	2.34	2.0	LC	0–7.5 mT	15	29.6	6.7	3.7	—	—	—	—	0.04
			HC	19–145 mT	113	236.3	−37.6	17.3	13.3	244.9	−36.3	13.9	—
DOM.d	1.61	3.1	LC	0–6 mT	12	34.3	16.8	5.5	—	—	—	—	0.27
			MC	6–17.5 mT	24	80.7	−30.2	30	—	—	—	—	—
			MC	17.5–32 mT	23	204.5	−62.6	25.6	48.9	303.4	−54.7	13.4	—
			HC*	32–145 mT	94	309.1	11	39	—	—	—	—	—
DOM.j	1.75	7.6	LC	0–28 mT	53	120.2	53.4	4.4	—	—	—	—	0.64
			MC	28–45 mT	18	200.8	75.4	18.8	7.9	189.8	69.9	9.2	—
			HC*	45–145 mT	81	149.7	38.7	49	—	—	—	—	—
DOM.k	3.28	6.9	LC	0–9.5 mT	19	66.1	22.6	4.9	—	—	—	—	0.24
			MC	9.5–24 mT	30	72.9	46.5	12.8	39.5	114	32.1	14.8	—
			HC*	24–145 mT	103	171.8	−30.6	42.3	—	—	—	—	—
DOM.l	3.50	5.8	LC	0–6 mT	12	35.6	11.7	2.6	—	—	—	—	0.33
			MC	6–28 mT	42	207	12.9	40.3	—	—	—	—	—
			HC	28–145 mT	98	100.4	−22.7	35.2	11.3	94.7	−15.5	21	—
DOM.m	1.71	4.8	LC	1–15.5 mT	30	45	29.7	10.6	37.9	57.5	50.1	19.8	0.22
			HC*	15.5–145 mT	120	119.8	54.2	44.4	—	—	—	—	—
DOM.g	1.78	2.0	LT	0–350°C	8	357.1	−23.2	20.2	—	—	—	—	—
			HT*	350–650°C	7	352.2	−37.9	33.8	—	—	—	—	—
DOM.ha**	1.13	3.0	LT	0–350°C	8	39.2	−9.1	8.2	—	—	—	—	—
			HT*	350–650°C	7	10.6	15.9	33.4	—	—	—	—	—

Table 1
Continued

Sample	Weight (mg)	Distance from fusion crust (mm)	Component	Range (mT or °C)	<i>N</i>	Declination (°)	Inclination (°)	MAD (°)	DANG (°)	Anchored declination (°)	Anchored inclination (°)	Anchored MAD (°)	NRM/ARM
DOM. hb**	2.23	3.1	LT	0–200°C	5	42.3	–9	7.4	–	–	–	–	–
			HT*	200–650°C	10	335.6	30.2	40.2	–	–	–	–	–
DOM. ia***	2.71	3.8	LT	0–350°C	8	34.8	–6.4	13.9	–	–	–	–	–
			HT*	400–600°C	5	198.8	–6.1	20.1	–	–	–	–	–
DOM. ib***	0.67	3.8	LT	0–350°C	8	34.8	–6.4	13.9	–	–	–	–	–
			HT*	400–600°C	5	171.5	8.8	27.1	–	–	–	–	–

Note. The first column shows the sample name, the second shows the weight (in mg) of the sample, the third shows the distance from the fusion crust (in mm; “fusion-crust” if the sample contained fusion crust), the fourth shows the name of the component (LC = low coercivity, MC = medium coercivity, HC = high coercivity, LT = low temperature and HT = high temperature), the fifth shows the range of levels/temperatures used in the PCA fit (in mT or °C), the sixth shows the number of data points in the PCA fit, the seventh, eighth, and ninth show the declination, inclination, and maximum angular deviation (MAD) for the fit without anchoring to the origin, the tenth shows the deviation angle (DANG) between anchored and non-origin-anchored fits, the eleventh, twelfth, and thirteenth show the origin-anchored declination, origin-anchored inclination, and origin-anchored MAD for the fits, and the fourteenth shows the NRM to ARM (AC field of 145 mT with a DC bias field of 50 μ T) ratio. * indicate non magnetized range; ** and *** show subsamples from one sample.

Because the non-fusion-crust samples contain CRMs, both the ARM and the IZZI methods cannot reliably reproduce in the laboratory the natural process by which the NRM was acquired by these samples. Therefore, knowledge of the ratio of CRM to ARM and CRM to thermal remanent magnetization (TRM) is required to obtain paleointensity estimates from these experiments. Unfortunately, these are poorly constrained. Previous studies determined a TRM to ARM ratio f' of 3.33 for magnetite and Fe-Ni bearing samples, which has an estimated 2σ that could be of at least a factor of 5 (Weiss & Tikoo, 2014). For alteration timescales of a year to millions of years, such as those experienced by carbonaceous chondrites (Dyl et al., 2012; Ganino & Libourel, 2020; Krot et al., 2006), TRM/CRM can be ~ 1 –2 (McClelland, 1996). For shorter alteration timescales ($\sim 10^3$ s), this ratio can be as large as ~ 5 –10 (McClelland, 1996). For this study, we assume that TRM \sim CRM and we use $f' = 3.33$ for the ARM method. We note that the paleointensities and recording limits described here are likely to be underestimations and future experiments are necessary to fully determine the CRM to ARM ratio as we discuss in Section 5.

We sought to estimate the minimum paleointensity that we could recover from our samples using the ARM method (Bryson et al., 2017; Tikoo et al., 2012). We determined this for each sample by applying a sequence of ARMs (AC field of 145 mT) with DC bias fields ranging from 1 to 10 μ T. We then attempted to retrieve these paleointensities using the ARM method described above (using an ARM bias field of 50 μ T) in the same coercivity range used to determine the paleointensity. We quantified the accuracy and precision of the retrieved paleointensity estimates with deviation of the retrieved magnetic field from the applied field (D') and the uncertainty of the retrieved field (E) metrics (Bryson et al., 2017; Tikoo et al., 2012). Again, we assumed $f' = 3.33$ such that the range of applied CRM-equivalent paleointensities were 0.3–3 μ T. For a given sample, we estimate the minimum paleointensity that can be recovered as the lowest value for which a sample presented $-0.5 < D' < 1$ and $E < 1$.

We also experimentally determined the viscous remanent magnetization (VRM) acquisition and decay rate of one of our samples from DOM 08006 to determine what fraction of the NRM could have been acquired through VRM. We exposed a previously demagnetized sample for 37 days in a terrestrial field of 46 μ T and measurements were taken periodically during this time. VRM decay was measured while the sample was kept inside a magnetically shielded room (~ 200 nT) for 14 days and measured periodically.

3. Results

3.1. ALHA77307

All AF-demagnetized samples contained a low coercivity (LC) component (blocked up to 58 mT) that had directions with overlapping MADs (Figure 1; Table 1). The fusion-crust samples also contained a high coercivity (HCf) component blocked between 26 and 410 mT (Figure 1). By comparison, further AF demagnetization of

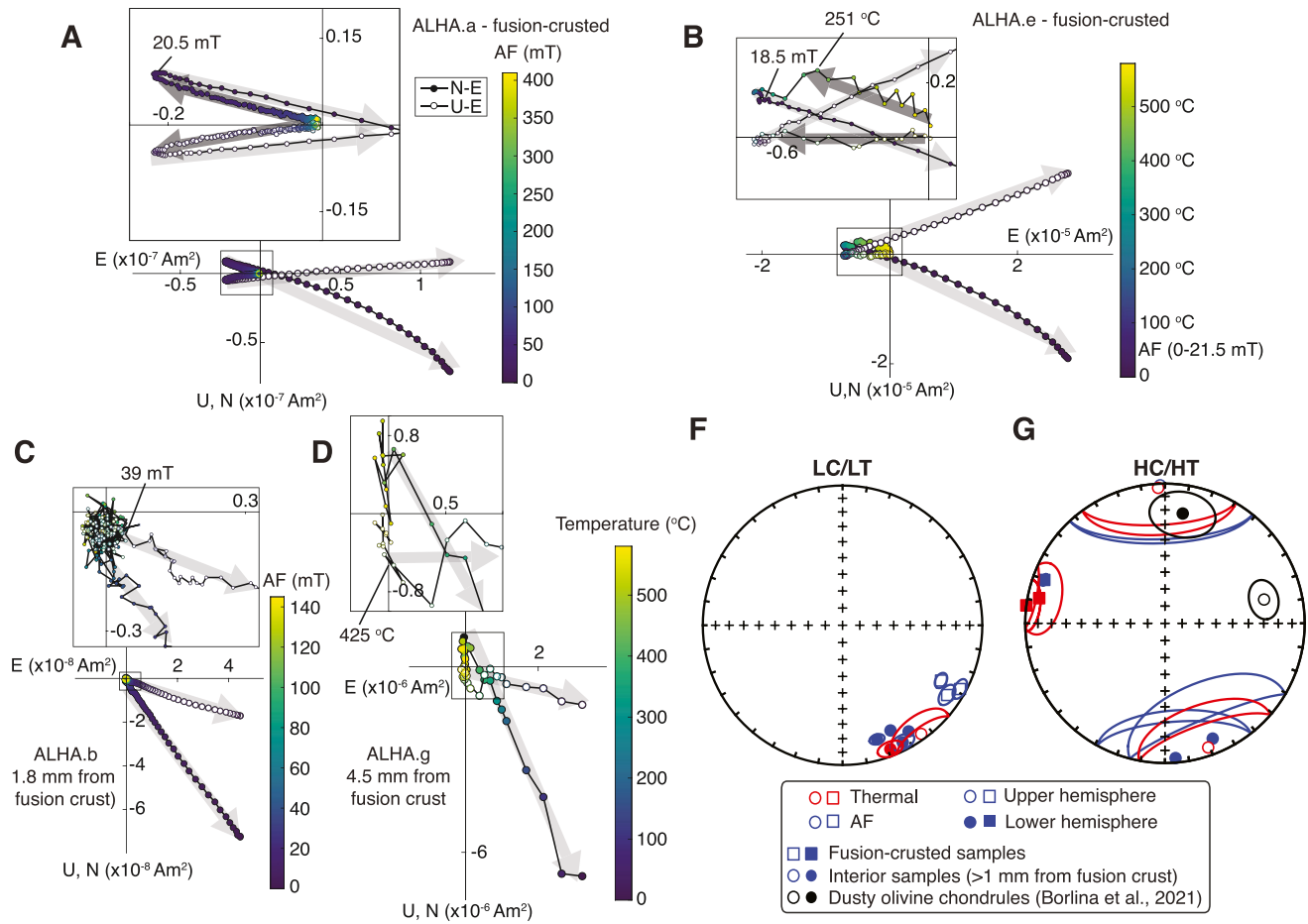


Figure 1. AF and thermal demagnetization of samples from ALHA77307. Selected orthographic projections of NRM vector endpoints during AF and thermal demagnetization for samples (a) ALHA.a, (b) ALHA.e, (c) ALHA.b, and (d) ALHA.g. Closed symbols show the north-east (N-E) projection of the magnetization and open symbols show the up-east (U-E) projection of the magnetization. Selected AF and thermal steps are labeled. (a) and (c) show AF demagnetization from fusion-crust and interior samples (>1 mm away from fusion crust), respectively. (b) and (c) show thermal demagnetization from fusion-crust and interior samples, respectively. (f)–(g) show equal area stereonet projections of the directions of low coercivity/low temperature (LC/LT) and high coercivity/high temperature (HC/HT) components from all samples measured from ALHA77307. Open and closed symbols represent upper and lower hemispheres, respectively. Red symbols show components from thermal demagnetization, while blue symbols show components from AF demagnetization. Squares show fusion-crust samples, while circles show interior samples. Black data points in equal area stereonet projections show the HC components from dusty olivine chondrules from Borlina et al. (2021).

the interior samples to 145 mT demonstrated that they contained little or no stable magnetization in this high coercivity (HC) range after removal of the LC component (Figure 1; Figure S1 in Supporting Information S1). PCA fits to the HC range for three of the five interior subsamples yield directions similar to the LC component despite large MADs and noisy demagnetization.

Using the ARM method, the fusion-crust samples yielded an apparent paleointensity of $358.5 \pm 15.8 \mu\text{T}$ (these and all other reported uncertainties are 2σ) for the LC component and a paleointensity of $26.7 \pm 0.8 \mu\text{T}$ for the HCf component (Figure S2 in Supporting Information S1). The presence of an LC component with clustered directions among all four samples and the high apparent paleointensity retrieved from the LC component suggest that ALHA77307 was exposed to contamination from a magnet (i.e., IRM) after atmospheric entry. We note that the fact that the fusion-crust samples were not completely IRM-remagnetized (i.e., they have both LC IRM overprint and the HCf component) and that the paleointensity of the HCf component has a strength similar to Earth's magnetic field implies that the HCf component is likely a TRM acquired during atmospheric entry. The presence of an HCf component in the fusion-crust samples and not in interior samples also demonstrates that ALHA77307 was not completely thermally remagnetized by atmospheric entry or IRM-remagnetized after landing. The fact that two subsamples presented LC-like direction for their HC fits may be because a small fraction of

grains demagnetizing in the HC range have residual IRM not demagnetized in the LC range, as may occur when none of the three AF axes are not coaligned with the IRM field direction (Stephenson, 1983).

The ARM method applied to the apparently nonmagnetized HC range of the interior samples (Figure S2 in Supporting Information S1) yielded a paleointensity of $2.2 \pm 0.9 \mu\text{T}$ (Table 2). Although the 2σ uncertainty does not formally encompass zero paleointensity, this may be due to residual undemagnetized IRM overprint of some grains in the HC range or spurious ARM acquired from the AF. In any case, the low paleointensity value and the lack of a unidirectional and stable component in the HC range (Figure S2 in Supporting Information S1) suggest that a weak or null field was present when ALHA77307 acquired its magnetic record. Figure 2 and Table 2 show that the interior sample (ALHA.d) can record fields $>0.9 \mu\text{T}$. We note that even though the HC components of the interior samples have high MADs, the means of two interior samples are similar to the direction of the LC component. As discussed above, this suggests that the presence of an IRM overprint could have implications for the HC range, specifically making it challenging to identify potential magnetic records in this range. If we ignore the interior samples that had HC components similar to the direction of the LC components, we have one sample (ALHA.c) that yielded a paleointensity of $1.5 \pm 0.5 \mu\text{T}$ and can record fields $>1.5 \mu\text{T}$ (Table 2).

Thermal demagnetization of a $50 \mu\text{T}$ ARM applied to two of the interior samples that were previously AF demagnetized shows that the magnetic remanence is carried by sulfide, magnetite (the main magnetic carrier; see Section 2.1.2), and Fe-metal, likely awaruite (Figure S3 in Supporting Information S1), consistent with the expected mineralogy of CO chondrites (Section 2.1.1).

The results of the IZZI protocol are presented in Table 3 and Figure S4 in Supporting Information S1. After the removal of the LC component from the fusion-crusted samples, we observed high temperature (HTf) components ($250\text{--}580^\circ\text{C}$) oriented close to the directions of the HCf components (Figure 1). The fusion-crusted samples successfully passed the PICRIT03 criteria, indicating minimum thermochemical alteration during laboratory heating. The paleointensities retrieved from the HTf components were of $13.9 \pm 4.7 \mu\text{T}$ and $13.9 \pm 5.4 \mu\text{T}$ (Table 3; Figure S4 in Supporting Information S1). These are within error of the ARM paleointensities retrieved from the HCf component given the uncertainties in the values of ARM/CRM and TRM/CRM. One interior sample (ALHA.g) had an LT component ($0\text{--}425^\circ\text{C}$) similar in direction to the LC components of the other samples followed by an origin-trending HT component ($425\text{--}580^\circ\text{C}$) oriented close to the direction of the laboratory field. The latter may have resulted from thermochemical alteration during the heating experiments (Figure 1d). The other interior sample (ALHA.h; LC removed with AF prior to the IZZI protocol) also had an LT component ($51\text{--}475^\circ\text{C}$) oriented in the direction of the LC components of the other samples (Figure S1d in Supporting Information S1). Due to thermochemical alteration during heating experiments, both interior samples fail multiple PICRIT03 alteration selection criteria (Table 3; Paterson et al., 2014), which implies that the HT component paleointensities of the interior samples cannot be reliably estimated.

In summary, the LC/LT component common to all samples is likely an IRM that did not completely overprint the sample, almost certainly acquired during sample handling. The HCf/HTf component, which is only present in the fusion-crusted samples, is consistent with magnetization acquired during heating from atmospheric entry in Earth's magnetic field. The lack of components, large MADs, and the fidelity tests among interior samples suggest that the ancient field environment was less than $0.9 \mu\text{T}$ when ALHA77307 acquired its magnetization. Nonetheless, the IRM overprint in the low coercivity range makes it challenging to obtain robust constraints from ALHA77307.

3.2. DOM 08006

All AF-demagnetized DOM 08006 samples from the interior had a common LC component blocked up to 28 mT (Figure 3 and Figure S5 in Supporting Information S1; Table 1). The fusion-crusted sample had a single origin-trending HCf component blocked up to 145 mT (Figure 3). Using the ARM method, we obtained a paleointensity of $39.5 \pm 0.4 \mu\text{T}$ for the HTf component of the fusion-crusted sample, consistent with Earth's magnetic field strength as recorded during atmospheric entry (Table 2; Figure 4).

Four interior samples had medium coercivity (MC) components with coercivities up to 45 mT (Figure 3), but no stable HC magnetization blocked beyond this. A fifth sample had an HC component between 19 and 145 mT (Figure S5a in Supporting Information S1). The remaining two samples did not carry any components blocked above 15 mT. PCA of the HC range yields scattered directions and MAD values $>40^\circ$ for most samples (Figure 3;

Table 2
Paleointensities From the ARM Experiment With Samples From ALHA77307 and DOM 08006

Sample	Distance from fusion crust (mm)	Range (mT)	<i>N</i>	ρ	Fit type	Paleofield (μ T)	95% conf int (μ T)	Recording limit (μ T)
ALHA.a	fusion crusted	0–10	20	1	OLS	358.5	15.8	–
		26–145	100	0.99	RMA	26.7	0.8	–
ALHA.b	7.7	0–10	20	0.99	OLS	206.9	10.2	–
		39–145	87	0.8	RMA	2	0.3	–
ALHA.c	3.2	0–9	18	0.99	OLS	247.7	16.3	–
		55–145	71	0.5	OLS	1.5	0.5	>1.5
ALHA.d	4.9	0–10	20	0.99	OLS	113.3	7.3	–
		55–145	71	0.54	OLS	3	0.6	>0.9
Mean						2.2	only high coercivity and no fusion crust	
Std. error						0.4		
95% conf. int						0.9		
DOM.a	fusion crusted	0–145	150	1	RMA	39.5	0.4	–
DOM.b	0.9	0–10	20	0.97	OLS	16.4	2.2	–
		10–145	131	0.14	OLS	0.1	0.1	>1.5
DOM.c	2.0	0–7.5	15	0.98	OLS	28	3.4	–
		19–145	113	0.97	RMA	4.1	0.2	>0.3
DOM.d	3.1	0–6	12	0.93	OLS	29.5	8.1	–
		6–17.5	24	0.94	RMA	5.4	0.8	–
		17.5–32	23	0.87	RMA	6.4	1.5	–
		32–145	94	–	OLS	–0.02	0.7	>3
DOM.j	7.6	0–28	53	1	RMA	18.5	0.6	–
		28–45	18	1	OLS	7.1	1.8	–
		45–145	81	0.27	OLS	0.8	0.6	>0.9
DOM.k	6.9	0–9.5	19	1	OLS	17.9	1.3	–
		9.5–24	30	0.97	RMA	5.7	0.5	–
		24–145	103	–	OLS	–0.3	0.2	>1.5
DOM.l	5.8	0–6	12	0.97	OLS	34.1	5.7	–
		28–145	98	0.83	RMA	3.4	0.4	>0.9
DOM.m	4.8	1–15.5	30	0.94	RMA	12.9	1.6	–
		15.5–145	120	0.3	OLS	0.3	0.2	>1.5
Mean						1.2	only high coercivity and no fusion crust	
Std. error						0.7		
95% conf. int						1.4		

Table 2
Continued

Sample	Distance from fusion crust (mm)	Range (mT)	<i>N</i>	ρ	Fit type	Paleofield (μ T)	95% conf int (μ T)	Recording limit (μ T)
					Mean	0.2	only high coercivity, no fusion crust, DOM.c and DOM.l not included	
					Std. error	0.2		
					95% conf. int	0.4		

Note. The first column shows the sample name, the second shows the distance from the fusion crust (in mm; “fusion-crust” if the sample contained fusion crust), the third shows the range of AF levels used in the paleointensity fit (in mT), the fourth shows the number of data points used in the paleointensity fit, the fifth shows the parametric correlation (ρ) between NRM and ARM datasets, the sixth shows the type of fit used to calculate the paleointensity (OLS = ordinary least squares; RMA = reduced major axis), the seventh shows the paleointensity (in μ T), the eighth shows the calculated 95% confidence interval of the paleointensity fit (in μ T), and the ninth shows the recording limit of the sample (in μ T) obtained from Figures 2 and 6. For each sample (ALHA77307 and DOM 08006) we calculated mean paleointensities, along with the standard error and the 95% confidence interval.

Table 1). The LC and MC components are likely associated with VRM and/or low temperature parent body thermochemical alteration. To assess this, we analyzed the VRM acquisition and decay properties of sample DOM.m following the AF demagnetization experiments. We measured a VRM acquisition rate of $1.15 \times 10^{-6} \text{ Am}^2 \text{ kg}^{-1} \mu\text{T}^{-1}$ and a VRM decay rate that was shallow at first ($\sim 10^3 \text{ s}$) with a decay rate of $2.06 \times 10^{-8} \text{ Am}^2 \text{ kg}^{-1} \mu\text{T}^{-1}$, followed by an increase in the decay rate to a value of $8.17 \times 10^{-7} \text{ Am}^2 \text{ kg}^{-1} \mu\text{T}^{-1}$ (Figure 5). Because Antarctic meteorites typically have terrestrial ages of a few tens of thousands of years (Jull, 2006) with some surviving for up to 2 million years, we estimate that $\sim 52\%$ of the NRM of the DOM.m could have been acquired in 10,000 years on the Earth's surface, consistent with the magnetic moment carried by the LC component.

The ARM method yielded a mean paleointensity of $1.2 \pm 1.4 \mu\text{T}$ for the HC range (Figure 4 and Figure S6 in Supporting Information S1; Table 2). Similar to the interior samples from ALHA77307, the lack of stable, unidirectional components in the HC range, the paleointensities within error of zero retrieved from the ARM method, and the demonstrated capacity for gaining ARM in the same nonmagnetized range (Figure 4 and Figure S6 in Supporting Information S1) indicate that a weak to null field was present when the magnetic record was acquired. We chose to not include DOM.c and DOM.l as part of our paleointensity analysis. DOM.c contains a well-constrained HC component (19–145 mT, MAD = 13.9°) that is not observed in any other sample and records a paleointensity of $4.1 \pm 0.2 \mu\text{T}$. DOM.l also contained an HC component (28–145 mT, MAD = 21°) with a distinct direction than that of DOM.c, which yields a paleointensity of $3.4 \pm 0.4 \mu\text{T}$, which is higher than its fidelity limit of $0.9 \mu\text{T}$ (Figure 6; Table 2). These records are not observed in any of the other subsamples. Even though magnetic directions of DOM.c and DOM.l are distinct, these could have been acquired at different times in the solar nebula. Nonetheless, because parent body alteration extends for periods of time in the order of millions of years (see Section 2) and there is no evidence for multiple alteration events in the parent body (Doyle et al., 2014), the magnetic record is likely to be an average of the magnetic field. We conclude that the records from DOM.c and DOM.l are due to the presence of large or highly magnetic chondrules and refractory inclusions in the bulk samples with pre-accretional magnetization and/or with spurious remanence acquired during AF demagnetization (Weiss et al., 2010).

Not including DOM.c and DOM.l results in a mean paleointensity of $0.2 \pm 0.4 \mu\text{T}$. The fidelity test for interior samples from DOM 08006 (Figure 6; Table 2) show that the sample with the best fidelity record is DOM.j, recording fields $>0.9 \mu\text{T}$. We conclude that the HC magnetic record was likely acquired in an environment with a paleointensity of $<0.9 \mu\text{T}$.

The thermal experiments identified LT components (blocked up to 350°C) in all samples whose direction is similar to the direction of the LC components (Figure 3). No components were observed blocked above 350°C , as indicated by the scattered directions and large MADs yielded by PCA fits (Figure 3; Table 1). The two samples on which we conducted the IZZI experiment failed multiple PICRIT03 alteration selection criteria. Thus, paleointensities and components direction are unlikely to be robust (Figure S7 in Supporting Information S1; Table 3).

In summary, the LC/LT/MC/MT components can be associated with low temperature parent body thermochemical alteration and/or VRM acquisition and the fidelity test indicates that the HC range of DOM 08006 recorded a field $<0.9 \mu\text{T}$.

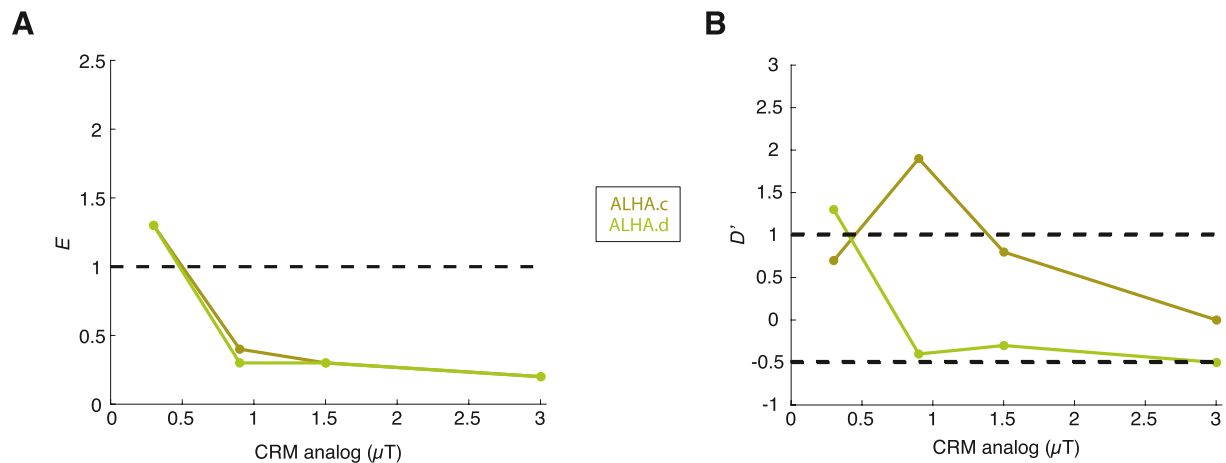


Figure 2. E and D' values calculated for samples from ALHA77307. Values below (a) and between (b) the dashed lines represent reliable paleomagnetic fidelities. The coercivity range, of each sample, used to calculate the paleointensities were used to calculate the E and D' values. The CRM analogs were calculated using $f = 3.33$ from ARMs (AC field of 145 mT) with DC bias fields of 10, 5, 3, and 1 μ T (estimated CRM-equivalent fields of 3, 1.5, 0.9, and 0.3 μ T).

4. Discussion

In the early solar system, there were at least four sources of magnetic fields that could conceivably have exceeded 0.9 μ T: the solar wind magnetic field, impact-generated fields, a parent body core dynamo magnetic field, and the solar nebula magnetic field. Below we discuss the implications of the magnetic record obtained from the CO chondrites and previous measurements for each one of these possibilities. We note that this discussion assumes that the magnetite is capable of having recorded a CRM during parent body alteration. We discuss in Section 5 why this might not be the case and future directions to address this.

4.1. Implications for the Solar Wind Magnetic Fields

Previous studies have discussed the possibility of the solar wind as a source of remanence recorded by the parent bodies of meteorites (Oran et al., 2018; O'Brien et al., 2020). MHD simulations indicate that the solar wind magnetic field could instantaneously have been amplified to a few μ T, but the time-averaged field that would be recorded as a CRM in our meteorites would be several orders of magnitude lower than this value (Oran

Table 3

Paleointensities and Calculated Paleomagnetic Criteria (PICRIT03 From (Paterson et al., 2014)) From the IZZI Experiment for ALHA77307 and DOM 08006

Sample	Distance from fusion crust (mm)	Range (°C)	N	Lab field direction (dec,inc) (°)	Paleofield (μ T)	95% conf int (μ T)	DRATS	f	β	q	CDRAT	Max. DRAT	Number of pTRM checks
ALHA.e	fusion crusted	400–580	13	(0,0)	13.9	4.7	5	1.1	0.3	2.8	5.1	17.8	6
ALHA.f	fusion crusted	400–580	13	(0,0)	13.9	5.4	0.5	1	0.4	2.3	0.5	7.8	6
ALHA.g	4.5	540–580	12	(0,0)	1.5	8.9	34.6	0.4	5.9	−0.1	51.9	23.4	6
ALHA.h	5.8	475–580	10	(0,0)	−7.3	10.2	3	1.5	1.4	−0.8	3.9	62.8	6
DOM.ia	3.8	0–350	8	(180,0)	23.1	20.7	35	2.5	0.9	2.2	30.4	17.1	3
		400–600	5		2.8	4.5	13	0.7	1.6	0.2	14.9	4.9	5
DOM.ib	3.8	0–350	8	(180,0)	23.1	20.7	35	2.5	0.9	2.2	30.4	17.1	3
		400–600	5		3.6	5.1	13	0.9	1.4	0.4	14.7	5.3	5

Note. The first column shows the sample name, the second shows the distance from the fusion crust (in mm; “fusion-crusted” if the sample contained fusion crust), the third shows the range of temperatures used in the paleointensity fit (in °C), the fourth shows the number of data points used in the fit, the fifth shows the direction of the laboratory field, the sixth shows the paleointensity (in μ T), the seventh shows the calculated 95% confidence interval of the paleointensity fit (in μ T), the eighth through thirteenth show the paleomagnetic parameters DRATS, f , β , q , CDRAT, and maximum DRAT from Paterson et al. (2014), and the fourteenth shows the number of pTRM checks conducted during the IZZI experiment.

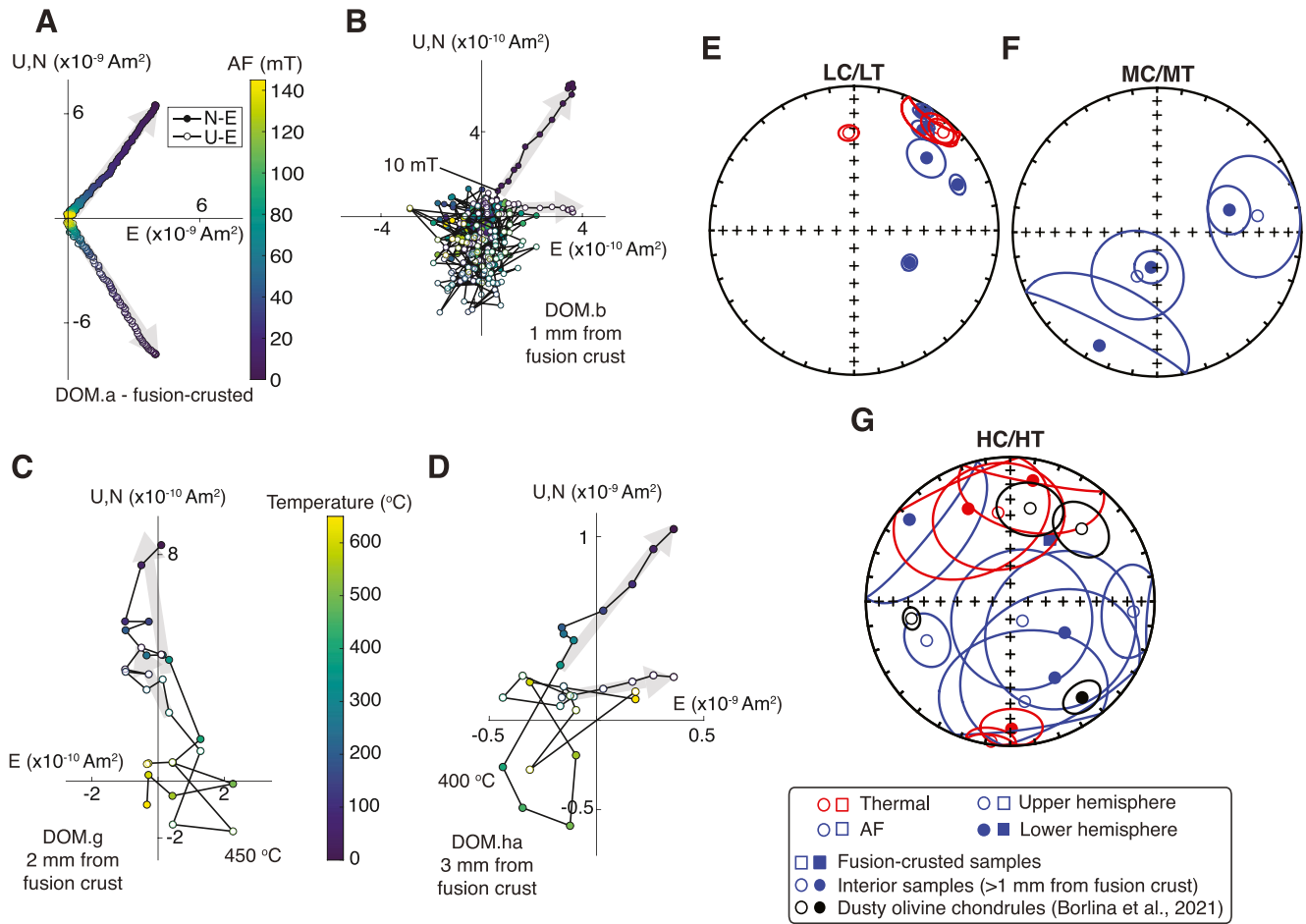


Figure 3. AF and thermal demagnetization of samples from DOM 08006. Selected orthographic projections of NRM vector endpoints during AF and thermal demagnetization for samples (a) DOM.a, (b) DOM.b, (c) DOM.g, and (d) DOM.ha. Closed symbols show the north-east (N-E) projection of the magnetization and open symbols show the up-east (U-E) projection of the magnetization. Selected AF and thermal steps are labeled. (a)–(b) show AF demagnetization from fusion-crusted and interior samples (>1 mm away from fusion crust), respectively. (c)–(d) show thermal demagnetization from interior samples. (e)–(g) show equal area stereonet projections with the directions of low coercivity/low temperature (LC/LT), medium coercivity/medium temperature (MC/MT), and high coercivity/high temperature (HC/HT) components from all samples measured from DOM 08006. Open and closed symbols represent upper and lower hemispheres, respectively. Red symbols show components from thermal demagnetization, while blue symbols show components from AF demagnetization. Squares show fusion-crusted samples, while circles show interior samples. Black data points in equal area stereonet projections show HC components from dusty olivine chondrules from Borlina et al. (2021).

et al., 2018). Our findings from CO chondrites place an upper limit to the time-averaged solar wind magnetic field of $<0.9 \mu\text{T}$, consistent with these studies.

4.2. Implications for Impact and Dynamos in Planetesimals

Planetesimals have been proposed to have sustained magnetic fields through different mechanisms. A planetesimal dynamo could have been generated by advection of an interior liquid metallic core (Sternberg & Crowley, 2013). Alternatively, magnetic fields could have been produced transiently during impacts (Weiss et al., 2010). Our records could imply that at the time that the magnetic record was acquired, fields with intensities $<0.9 \mu\text{T}$ (due to a dynamo, crustal remanence from a previous dynamo, or impact-generated field) were present on the CO parent body. Weak fields such as the upper limit of our measurements are within the values predicted by core dynamo scaling laws (Weiss et al., 2010). Furthermore, models of thermal convection-driven dynamos suggest that field generation could start by ~ 4.5 – 5 Myr after CAI-formation (Bryson et al., 2019), relatively close to the timing of magnetic acquisition of our samples. In summary, any magnetic field on the parent body at the time of CO magnetization was weaker than $<0.9 \mu\text{T}$.

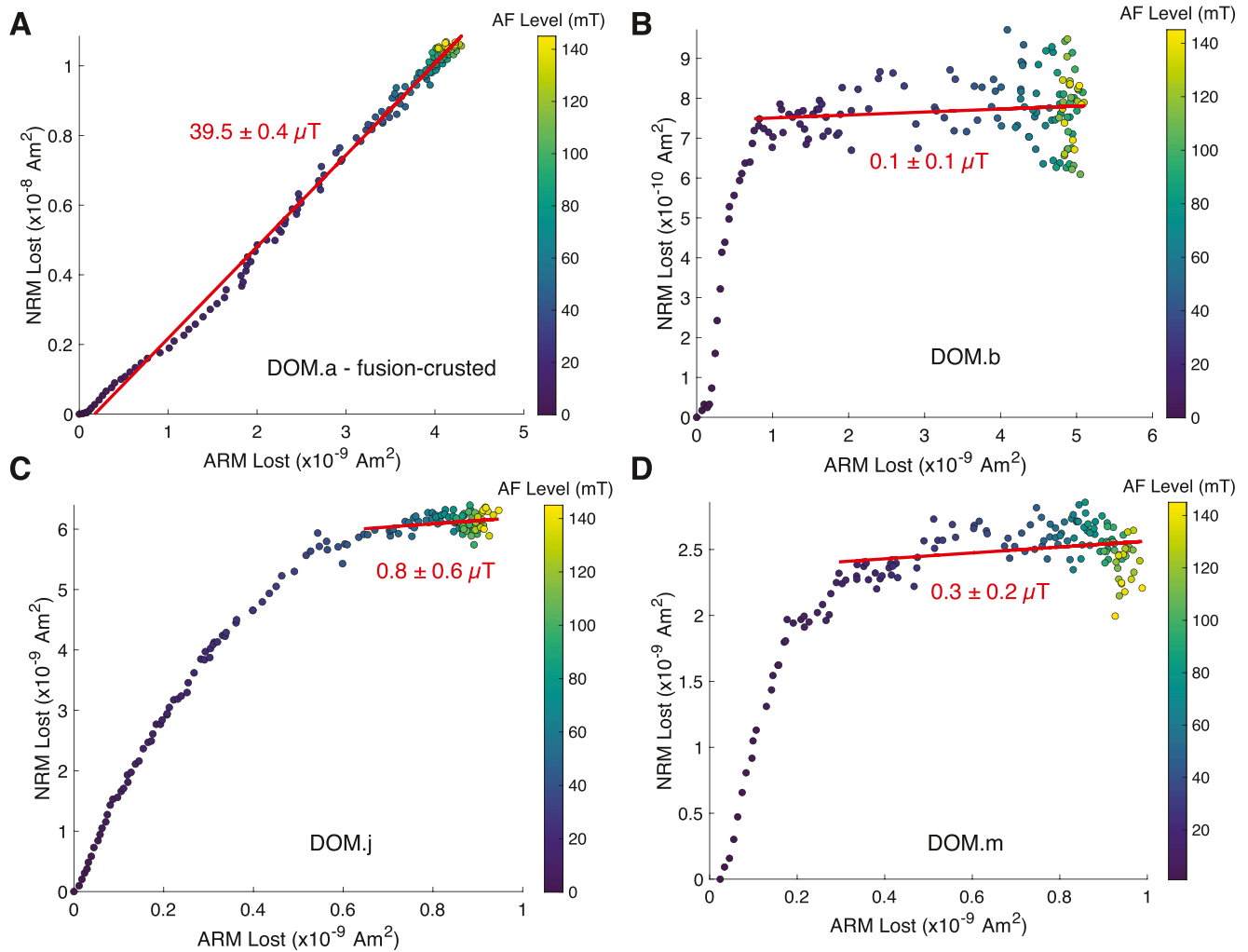


Figure 4. ARM paleointensity experiments for the selected samples (a) DOM.a, (b) DOM.b, (c) DOM.j, and (d) DOM.m from DOM 08006. Shown is NRM lost during stepwise AF demagnetization up to 145 mT and ARM lost during AF demagnetization up to 145 mT of an ARM (AC field of 145 mT with a DC bias field of 50 μ T). Paleointensities ($f' = 3.33$) and their 95% confidence intervals are reported. The red lines represent the range of coercivities used to calculate the fit.

4.3. Solar Nebular Magnetic Fields and Implications for the Dissipation of PPDs and Planetary Formation

Previous measurements support the presence of nebular fields in the early solar system (Borlina et al., 2021; Cournede et al., 2015; Fu et al., 2014, 2021). The youngest record of the solar nebula in the inner solar system comes from LL chondrules at 2.03 ± 0.81 Myr after CAI formation (Fu et al., 2014; Weiss et al., 2021), and the youngest record in the outer solar system comes from the CM chondrites at $3.9^{+0.4}_{-0.5}$ Myr after CAI-formation (Cournede et al., 2015; Fujiya et al., 2012). We note that I-Xe ages for the CMs have been reported as 2.9 ± 0.39 Myr after CAI-formation in the form of an abstract (Pravdivtseva et al., 2013) and recent ^{53}Mn - ^{53}Cr ages support a younger alteration time of $3.9^{+0.4}_{-0.5}$ Myr after CAI-formation (Fujiya et al., 2012). Figure 7 shows the results of the CO chondrites in context with those of previous studies (Fu et al., 2014, 2020, 2021; Biersteker et al., 2019; Borlina et al., 2021; Bryson et al., 2017, 2020; Cournede et al., 2015; Gattacceca et al., 2016; Wang et al., 2017; Weiss et al., 2017). We present in Figure 7a magnetic field models as a function of the distance from the Sun. Shown are three sets of curves, each assuming magnetic fields drove accretion at rates ranging from 10^{-7} to $10^{-9} M_{\odot} \text{ year}^{-1}$ as typically observed for actively accreting young stellar objects (Hartmann et al., 1998; Weiss et al., 2021). The first and second curves assume radial-azimuthal and vertical-azimuthal magnetic field stresses driving accretion in the case when the nebular field and the disk angular momentum are aligned, while the third curve assumes vertical-azimuthal stresses when the nebular field and the disk rotation are anti-aligned. Recent

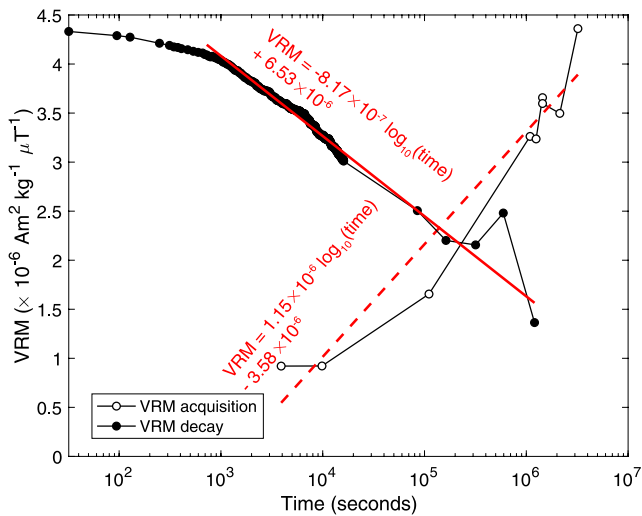


Figure 5. VRM acquisition and decay over a period of ~40 days of DOM.m, a 1.71 mg sample from DOM 08006. Closed symbols show measurements of the VRM decay experiment, open symbols show measurements of the VRM acquisition experiment, solid line shows linear fit of the VRM decay experiment, and dashed line shows linear fit of the VRM acquisition experiment.

studies have supported the presence of magnetic inhomogeneities in the early solar system (Borlina et al., 2021; Fu et al., 2021), which suggest that magnetic fields might not decay monotonically as proposed by theoretical models of solar nebula magnetic fields.

Measurements from dusty olivine chondrules in LL ordinary chondrites (Fu et al., 2014) are consistent with predictions from magnetically driven accretion at rates between 10^{-8} and 10^{-7} M_{\odot} year $^{-1}$ and provide lower limits to the accretion rate when compared to that reported by Borlina et al. (2021) from dusty olivine chondrules in CO chondrites. Comparing the accretion rate inferred from the lower limit of the paleointensity from the LL chondrules (Fu et al., 2014) to the models shown in Figure 7a, we obtain a value of $\sim 10^{-8}$ M_{\odot} year $^{-1}$. This model assumes an aligned configuration between the magnetic field and rotation of the disk. Under this configuration, a field of ~ 10 μ T would suggest that the solar nebula was still present in the outer solar system. Comparing the CO and CV bulk magnetic records with models that assume accretion rates $>10^{-8}$ M_{\odot} year $^{-1}$, we observe that the upper limits from this study (<0.9 μ T) and that of Kaba (<0.3 μ T) fall below the expected magnetic models by an order of magnitude. Assuming that accretion is magnetically mediated and that the magnetic field decayed smoothly in the early solar system, the upper limits on the paleointensities of the CO and CV chondrites suggest an absence of a nebula in the outer solar system nebula.

^{53}Mn - ^{53}Cr ages of fayalite from the CV3 Asuka 881317 indicate an alteration age of $4.2^{+0.8}_{-0.7}$ Myr after CAI formation (Doyle et al., 2014), which is within

the error of the I-Xe age from Kaba of 4.50 ± 1.66 Myr after CAI formation (Pravdivtseva et al., 2013). We note that the Kaba's ^{53}Mn - ^{53}Cr age reported in Gattacceca et al. (2016) used the San Carlos olivine standard that needs to be corrected in future measurements (Doyle et al., 2014). Instead, we adopt the ^{53}Mn - ^{53}Cr ages of fayalite from the CV3 Asuka 881317 of $4.2^{+0.8}_{-0.7}$ Myr after CAI formation as the Kaba alteration age (Figure 7b). Together, the CV and CO magnetic data suggest the dissipation of the outer solar system solar nebula by 2.7–5 Myr after CAI-formation, with the CV magnetic record providing the most well-constrained evidence for the dissipation of the nebula in the outer solar system of ~ 4.2 Myr after CAI-formation. This is broadly consistent with the recent models that suggest that chondrules from the CB carbonaceous chondrites Gujba and Hammadah al Hamra 237, which are thought to have formed at $4.6^{+0.5}_{-0.5}$ Myr after CAI formation and $4.5^{+0.9}_{-0.9}$ after CAI formation, respectively, as a result of high velocity impact between planetesimals in an environment where the nebular gas had already

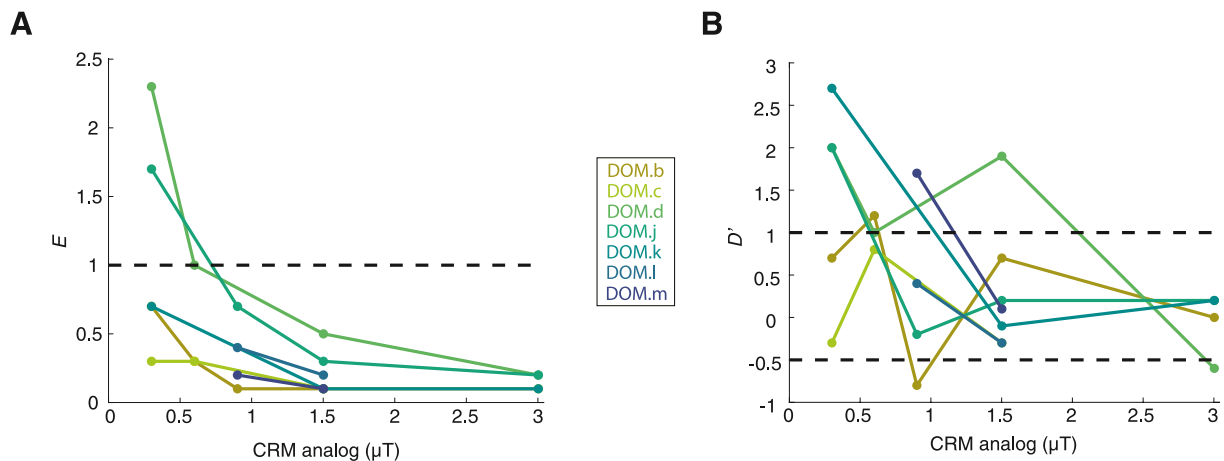


Figure 6. E and D' values calculated for samples from DOM 08006. Values below (a) and between (b) the dashed lines represent reliable paleomagnetic fidelities. The coercivity range, of each sample, used to calculate the paleointensities were used to calculate the E and D' values. The CRM analogs were calculated using $f' = 3.33$ from ARMs (AC field of 145 mT) with DC bias fields of 10, 5, 3, and 1 μ T (estimated CRM-equivalent fields of 3, 1.5, 0.9, and 0.3 μ T).

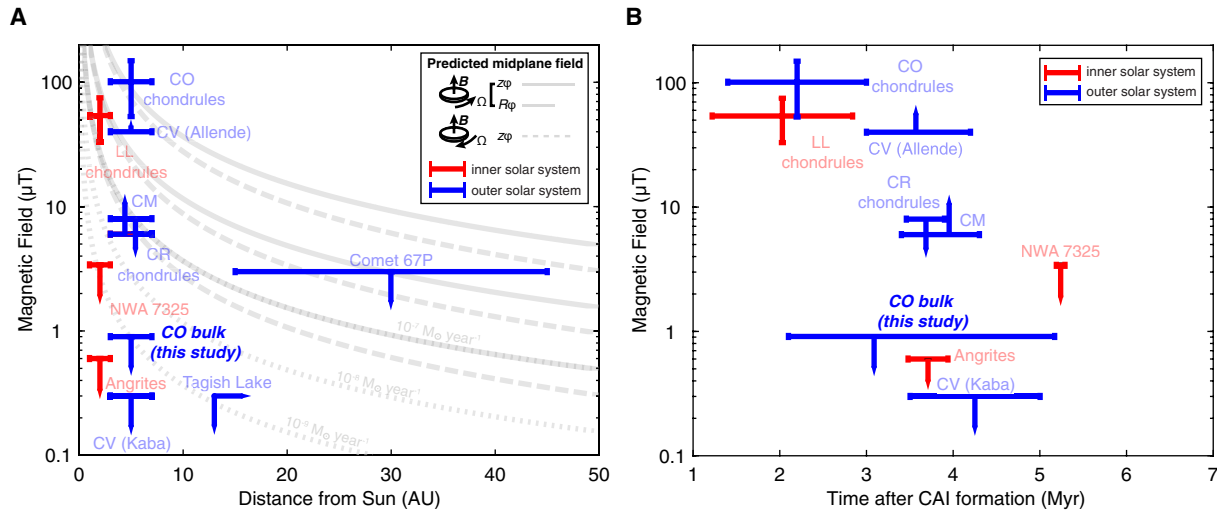


Figure 7. Summary of previous paleomagnetic studies along with results from this study and models of the magnetic field from the solar nebula. Points show paleomagnetic constraints from LL chondrules (Fu et al., 2014), CO chondrules (Borlina et al., 2021), bulk NWA 7325 achondrites (Weiss et al., 2017), bulk Angrites (Wang et al., 2017), bulk CV (Kaba) chondrites (Gattacceca et al., 2016), Fe-sulfides in CV (Allende) (Fu et al., 2021), CR chondrules (Fu et al., 2020), Rosetta observations of comet 67P Cheryumov Gerasimenko (Biersteker et al., 2019), and this study. Red symbols show samples that are likely from the inner solar system (<3 AU) and blue symbols show samples that are likely from the outer solar system (>3 AU). (a) Solid lines show predicted midplane magnetic field: solid lines show field due to vertical Maxwell stress ($z\phi$; Equation 16 of Bai and Goodman (2009)) and dashed lines show field due to radial Maxwell stress ($R\phi$; Equation 7 of Bai and Goodman (2009)), both assuming the nebular magnetic field and sense of disk rotation are aligned. Dotted lines show the field due to vertical Maxwell stress ($z\phi$; Equation 7 of Bai and Goodman (2009)), assuming nebular magnetic field and sense of disk rotation are anti-aligned (radial component cancels out for this case). All curves were calculated assuming accretion rates of 10^{-9} (bottom curve), 10^{-8} (middle curve), and $10^{-7} \text{ M}_{\odot} \text{ year}^{-1}$ (top curve). (b) Points show paleomagnetic constraints from (a) as a function of age.

dissipated (Krot et al., 2005) and with simulations of these impacts that indicate that the nebula dissipated by ~ 5 Myr after CAI formation (Johnson et al., 2016).

We can now establish the dissipation time of the solar nebula between the inner and outer solar system as well as within the outer solar system. Magnetic measurements suggest that the inner solar nebula dissipated by 3.71 ± 0.23 Myr after CAI formation (Wang et al., 2017; Weiss et al., 2021). Comparing the angrite age with that of the CV chondrites would suggest that the solar nebula dissipated within <1.5 Myr between the two reservoirs. If, independently, we compare the CM chondrite age with that of the CV chondrites, we obtain a dispersal time in the outer solar system solar nebula of <1.6 Myr after the CM magnetic record. These two upper limits on the differential dissipation time between and within the reservoirs suggest a rapid dissipation of the disk: together with the evidence that the disk existed for at least ~ 3 Myr, it supports a dual-timescale evolution of the solar system PPD. Models suggest that a two-timescale evolution of the disk is consistent with magnetically driven and/or photoevaporative winds predominately driving PPD dissipation (Armitage et al., 2013; Clarke et al., 2001; Shadmehri & Ghoreyshi, 2019) with potential influence of external photoevaporation aided by other stars (Concha-Ramírez et al., 2019).

Finally, the dissipation of the disk sets the limit for the accretion of gas to the gas giants (Weiss & Bottke, 2021). Thus, if we take the age of the CVs as the first evidence for the dissipation of the solar nebula in the outer solar system, that indicates that the gas giants stopped accreting mass sometime between 3.5 and 5 Myr after CAI formation.

5. Future Directions for Solar Nebula Paleomagnetism

While previous measurements (Cournede et al., 2015; Fu et al., 2021; Gattacceca et al., 2016) and those reported in this study can potentially provide important information about the lifetime of the solar nebula, two key aspects that are fundamental to obtaining robust records of the solar nebula magnetic field are largely unconstrained. First, additional high-precision ages from meteorites are necessary. Determining when alteration occurred in various meteorite parent bodies is crucial to establish when CRMs may have been acquired. Future studies that include age measurements of the alteration products in the meteorites (ideally dating the formation of the ferromagnetic

minerals of interest), including in CO chondrites, will be able to provide the precision necessary to establish more reliable timing of the solar nebula dispersal.

Second, as briefly discussed in Section 2.2, the CRM to ARM ratio for magnetite that formed during aqueous alteration of metal is undetermined. While chondrules and refractory inclusions likely acquired TRMs due to their pre-accretionary thermal histories, the magnetic record of bulk aqueously altered samples is usually carried in the form of CRMs. Unfortunately, very little is known about the mechanism of CRM acquisition during parent body alteration and how it can affect the recovered paleointensity. A recent study suggests that magnetite can form through different pathways in chondrites (Sridhar et al., 2021). Magnetite grains in most CM and CO chondrites likely formed through pseudomorphic replacement of metal, while magnetite in frambooids and plaquettes, which are found in comparatively high abundance in several chondrites, including the CM Paris, are thought to have formed through the dissolution of sulfide and precipitation of magnetite in these exotic morphologies. For the case that magnetite forms through replacement of metal, previous studies of alteration pseudomorphic reactions in terrestrial samples have observed that certain minerals can inherit the NRM carried by the precursor phase (Heider & Dunlop, 1987; Jiang et al., 2017). Because Fe-Ni metal across a bulk chondrite subsample is expected to carry a nonuniform remanence (because it will carry several non-unidirectional pre-accretionary remanences), it is possible that the absence of a remanence recorded by magnetite corresponds to a signal inherited from the metal. This could fundamentally impact the paleointensities obtained from CRMs carried by magnetite in CM chondrites (Cournede et al., 2015), CV chondrites (Fu et al., 2021; Gattacceca et al., 2016), and CO chondrites in this study. For the CMs, for example, the lack of HT components that demagnetize between the Curie temperatures of pyrrhotite and magnetite in most CM chondrites from Cournede et al. (2015) was interpreted to be due to alteration during laboratory heating. A second interpretation is that the magnetite inherited the remanence from its parent metal and, as a result, does not contain an HT component associated with magnetite. This interpretation is consistent with pyrrhotite in CM chondrites carrying a CRM, indicating that a field was seemingly present at some point during the alteration sequence of these meteorites, but there being no record of this remanence in the magnetite among most meteorites in this group. Notably, the magnetite in Paris does appear to carry a CRM, which is consistent with this meteorite containing a large proportion of magnetite frambooids and plaquettes that are likely to have recorded more traditional CRMs as the grains in these morphologies grew through their blocking volumes as they were precipitated. This interpretation could also explain the absence of a remanence in the CV Kaba at temperatures above the peak metamorphic temperature reached on the parent body (Gattacceca et al., 2016). This would suggest that the absence of a remanence may in fact not reflect the dissipation of the disk and its associated field but instead, the inability of magnetite to record a remanence when it forms through aqueous alteration of metal. To determine whether robust records of the solar nebula can in fact be recovered from bulk samples of aqueously altered chondrites, it is crucial to conduct experimental work to determine how magnetite in different families of chondrites could acquire CRMs.

6. Conclusions

We report paleomagnetic measurements of bulk samples from the CO chondrites ALHA77307 and DOM 08006. If magnetite could have recorded ambient fields during parent body alteration, the CO chondrite records indicate that the ambient field was $<0.9 \mu\text{T}$. Combining these results with previous paleomagnetic measurements, we suggest that the nebular gas in the carbonaceous chondrite region ($\sim 3\text{--}7$ AU) dissipated within 3.5–5 Myr after CAI-formation. Comparing the time of the dissipation of the nebula in the outer solar system with that from the inner solar system indicates that the difference in dissipation ages between the two reservoirs was <1.5 Myr. This supports a dual-timescale evolution of the solar system PPD, consistent with magnetically driven winds and/or photoevaporation as processes that mediated the dissipation of the solar system PPD. Additionally, the end of the solar nebula indicated that the gas giants stopped accreting by 3.5–5 Myr after CAI-formation. We also highlight issues in using magnetite in bulk carbonaceous chondrites to determine nebula field records and the future work necessary for such records to be acquired, as well as obtaining more ages from alteration products to obtain high-resolution temporal records from the nebula. We also discuss how there is a possibility that paleomagnetic measurements of carbonaceous chondrites that have been interpreted as evidence for the absence of a field in the solar nebula, including this study, might be a result of nonideal magnetic acquisition during parent body alteration. Overall, future experimental work to understand the mechanisms of CRM acquisition in parent bodies is critical to reliably obtain records of the solar nebula.

Data Availability Statement

All data needed to evaluate the conclusions in the paper can be found through the Magnetism Information Consortium (MagIC) Database: [doi:10.7288/V4/MAGIC/19362](https://doi.org/10.7288/V4/MAGIC/19362) (Borlina et al., 2022).

Acknowledgments

We thank E. Lima for helpful discussions. C.S.B. and B.P.W. thank the NASA Discovery Program (contract NNM16AA09C) and Thomas F. Peterson, Jr. for support.

References

- Alexander, C. M. O., Greenwood, R. C., Bowden, R., Gibson, J. M., Howard, K. T., & Franchi, I. A. (2018). A multi-technique search for the most primitive CO chondrites. *Geochim. Cosmochim. Acta*, astrophysical implications of extraterrestrial materials: A special issue for ernst K. Zinner, 221, 406–420. <https://doi.org/10.1016/j.gca.2017.04.021>
- Alexander, R. D., Clarke, C. J., & Pringle, J. E. (2006). Photoevaporation of protoplanetary discs – I. Hydrodynamic models. *Monthly Notices of the Royal Astronomical Society*, 369(1), 216–228. <https://doi.org/10.1111/j.1365-2966.2006.10293.x>
- Armitage, P. J., & Kley, W. (2019). *From protoplanetary disks to planet formation, saas-fee advanced course*. Springer-Verlag. <https://doi.org/10.1007/978-3-662-58687-7>
- Armitage, P. J., Simon, J. B., & Martin, R. G. (2013). Two timescale dispersal of magnetized protoplanetary disks. *The Astrophysical Journal*, 778(1), L14. <https://doi.org/10.1088/2041-8205/778/1/L14>
- Bai, X. (2016). Toward a global evolutionary model of protoplanetary disks. *The Astrophysical Journal*, 821(2), 80. <https://doi.org/10.3847/0004-637x/821/2/80>
- Bai, X. N., & Goodman, J. (2009). Heat and dust in active layers of protostellar disks. *The Astrophysical Journal*, 701(1), 737–755. <https://doi.org/10.1088/0004-637x/701/1/737>
- Biersteker, J. B., Weiss, B. P., Heinisch, P., Herčík, D., Glassmeier, K.-H., & Auster, H.-U. (2019). Implications of Philae magnetometry Measurements at comet 67P/Churyumov–Gerasimenko for the nebular field of the outer solar system. *The Astrophysical Journal*, 875(1), 39. <https://doi.org/10.3847/1538-4357/ab0f2a>
- Bonal, L., Bourlot-Denise, M., Quirico, E., Montagnac, G., & Lewin, E. (2007). Organic matter and metamorphic history of CO chondrites. *Geochimica et Cosmochimica Acta*, 71(6), 1605–1623. <https://doi.org/10.1016/j.gca.2006.12.014>
- Bonal, L., Quirico, E., Flandinet, L., & Montagnac, G. (2016). Thermal history of type 3 chondrites from the Antarctic meteorite collection determined by Raman spectroscopy of their polyaromatic carbonaceous matter. *Geochimica et Cosmochimica Acta*, 189, 312–337. <https://doi.org/10.1016/j.gca.2016.06.017>
- Borlina, C. S., Weiss, B. P., Bryson, J. F. J., Bai, X.-N., Lima, E. A., Chatterjee, N., & Mansbach, E. N. (2021). Paleomagnetic evidence for a disk substructure in the early solar system. *Science Advances*, 7(42), eabj6928. <https://doi.org/10.1126/sciadv.abj6928>
- Borlina, C. S., Weiss, B. P., Bryson, J. F. J., Bai, X.-N., Lima, E. A., Chatterjee, N., & Mansbach, E. N. (2022). *Lifetime of the outer solar system nebula from carbonaceous chondrites, Magnetism Information Consortium (MagIC)*. <https://doi.org/10.7288/V4/MAGIC/19362>
- Brasser, R., & Mojzsis, S. J. (2020). The partitioning of the inner and outer Solar System by a structured protoplanetary disk. *Nature Astronomy*, 4(5), 492–499. <https://doi.org/10.1038/s41550-019-0978-6>
- Bryson, J. F. J., Neufeld, J. A., & Nimmo, F. (2019). Constraints on asteroid magnetic field evolution and the radii of meteorite parent bodies from thermal modelling. *Earth and Planetary Science Letters*, 521, 68–78. <https://doi.org/10.1016/j.epsl.2019.05.046>
- Bryson, J. F. J., Weiss, B. P., Harrison, R. J., Herrero-Albillos, J., & Kronast, F. (2017). Paleomagnetic evidence for dynamo activity driven by inward crystallisation of a metallic asteroid. *Earth and Planetary Science Letters*, 472, 152–163. <https://doi.org/10.1016/j.epsl.2017.05.026>
- Bryson, J. F. J., Weiss, B. P., Lima, E. A., Gattacceca, J., & Cassata, W. S. (2020). Evidence for asteroid scattering and distal solar system solids from meteorite paleomagnetism. *The Astrophysical Journal*, 892(2), 126. <https://doi.org/10.3847/1538-4357/ab7cd4>
- Clarke, C. J., Gendrin, A., & Sotomayor, M. (2001). The dispersal of circumstellar discs: The role of the ultraviolet switch. *Monthly Notices of the Royal Astronomical Society*, 328(2), 485–491. <https://doi.org/10.1046/j.1365-8711.2001.04891.x>
- Concha-Ramírez, F., Wilhelm, M. J. C., Portegies Zwart, S., & Haworth, T. J. (2019). External photoevaporation of circumstellar discs constrains the time-scale for planet formation. *Monthly Notices of the Royal Astronomical Society*, 490(4), 5678–5690. <https://doi.org/10.1093/mnras/stz2973>
- Cournede, C., Gattacceca, J., Gounelle, M., Rochette, P., Weiss, B. P., & Zanda, B. (2015). An early solar system magnetic field recorded in CM chondrites. *Earth and Planetary Science Letters*, 410, 62–74. <https://doi.org/10.1016/j.epsl.2014.11.019>
- Davidson, J., Alexander, C. M. O., Stroud, R. M., Busemann, H., & Nittler, L. R. (2019). Mineralogy and petrology of dominion range 08006: A very primitive CO3 carbonaceous chondrite. *Geochimica et Cosmochimica Acta*, 265, 259–278. <https://doi.org/10.1016/j.gca.2019.08.032>
- DeMeo, F. E., & Carry, B. (2014). Solar System evolution from compositional mapping of the asteroid belt. *Nature*, 505(7485), 629–634. <https://doi.org/10.1038/nature12908>
- Desch, S. J., Kalyaan, A., & Alexander, C. M. O. (2018). The effect of Jupiter's formation on the distribution of refractory elements and inclusions in meteorites. *The Astrophysical Journal - Supplement Series*, 238(1), 11. <https://doi.org/10.3847/1538-4365/aad95f>
- Doyle, P. M., Jogo, K., Nagashima, K., Krot, A. N., Wakita, S., Ciesla, F. J., & Hutcheon, I. D. (2014). Early aqueous activity on the ordinary and carbonaceous chondrite parent bodies recorded by fayalite. *Nature Communications*, 6(1), 7444. <https://doi.org/10.1038/ncomms8444>
- Dullemond, C. P., & Dominik, C. (2005). Dust coagulation in protoplanetary disks: A rapid depletion of small grains. *Astronomy & Astrophysics*, 434(3), 971–986. <https://doi.org/10.1051/0004-6361:20042080>
- Dunlop, D. J. (2002). Theory and application of the Day plot (Mrs/Ms versus Hcr/Hc) - 2. Application to data for rocks, sediments, and soils. *Journal of Geophysical Research*, 107, EPM5-1–EPM5-15.
- Dunlop, D. J., & Özdemir, O. (1997). *Rock magnetism: Fundamentals and frontiers, cambridge studies in magnetism*. Cambridge University Press.
- Dyl, K. A., Bischoff, A., Ziegler, K., Young, E. D., Wimmer, K., & Bland, P. A. (2012). Early solar system hydrothermal activity in chondritic asteroids on 1–10-year timescales. *Proceedings of the National Academy of Sciences of the United States of America*, 109(45), 18306–18311. <https://doi.org/10.1073/pnas.1207475109>
- Ercolano, B., & Pascucci, I. (2017). The dispersal of planet-forming discs: Theory confronts observations. *Royal Society Open Science*, 4, 170114. <https://doi.org/10.1098/rsos.170114>
- Fu, R. R., Kehayias, P., Weiss, B. P., Schrader, D. L., Bai, X.-N., & Simon, J. B. (2020). Weak magnetic fields in the outer solar nebula recorded in CR chondrites. *Journal of Geophysical Research: Planets*, 125(5), e2019JE006260. <https://doi.org/10.1029/2019JE006260>
- Fu, R. R., Volk, M. W. R., Bilardello, D., Libourel, G., Lesur, G. R. J., & Dor, O. B. (2021). The fine-scale magnetic history of the allende meteorite: Implications for the structure of the solar nebula. *AGU Advances*, 2(3), e2021AV000486. <https://doi.org/10.1029/2021AV000486>

- Fu, R. R., Weiss, B. P., Lima, E. A., Harrison, R. J., Bai, X.-N., Desch, S. J., et al. (2014). Solar nebula magnetic fields recorded in the Semarkona meteorite. *Science*, 346(6213), 1089–1092. <https://doi.org/10.1126/science.1258022>
- Fujiya, W., Sugiura, N., Hotta, H., Ichimura, K., & Sano, Y. (2012). Evidence for the late formation of hydrous asteroids from young meteoritic carbonates. *Nature Communications*, 3(1), 627. <https://doi.org/10.1038/ncomms1635>
- Ganino, C., & Libourel, G. (2020). Fumarolic-like activity on carbonaceous chondrite parent body. *Science Advances*, 6(27), eabb1166. <https://doi.org/10.1126/sciadv.abb1166>
- Gattacceca, J., & Rochette, P. (2004). Toward a robust normalized magnetic paleointensity method applied to meteorites. *Earth and Planetary Science Letters*, 227(3–4), 377–393. <https://doi.org/10.1016/j.epsl.2004.09.013>
- Gattacceca, J., Weiss, B. P., & Gounelle, M. (2016). New constraints on the magnetic history of the CV parent body and the solar nebula from the Kaba meteorite. *Earth and Planetary Science Letters*, 455, 166–175. <https://doi.org/10.1016/j.epsl.2016.09.008>
- Gorti, U., Liseau, R., Sándor, Z., & Clarke, C. (2016). Disk dispersal: Theoretical understanding and observational constraints. *Space Science Reviews*, 205(1–4), 125–152. <https://doi.org/10.1007/s11214-015-0228-x>
- Grossman, J. N., & Brearley, A. J. (2005). The onset of metamorphism in ordinary and carbonaceous chondrites. *Meteoritics & Planetary Sciences*, 40(1), 87–122. <https://doi.org/10.1111/j.1945-5100.2005.tb00366.x>
- Haisch, K. E., Lada, E. A., & Lada, C. J. (2001). Disk frequencies and lifetimes in young clusters. *The Astrophysical Journal*, 553(2), L153–L156. <https://doi.org/10.1086/320685>
- Hartmann, L., Calvet, N., Gullbring, E., & D'Alessio, P. (1998). Accretion and the evolution of T Tauri disks. *The Astrophysical Journal*, 495(1), 385–400. <https://doi.org/10.1086/305277>
- Heider, F., & Dunlop, D. J. (1987). Two types of chemical remanent magnetization during the oxidation of magnetite. *Physics of the Earth and Planetary Interiors*, 46(1–3), 24–45. [https://doi.org/10.1016/0031-9201\(87\)90169-5](https://doi.org/10.1016/0031-9201(87)90169-5)
- Hernández, J., Hartmann, L., Megeath, T., Gutermuth, R., Muzerolle, J., Calvet, N., et al. (2007). A Spitzer Space Telescope study of disks in the young σ Orionis cluster. *The Astrophysical Journal*, 662(2), 1067–1081. <https://doi.org/10.1086/513735>
- Herdon, J. M., Rowe, M. W., Larson, E. E., & Watson, D. E. (1976). Thermomagnetic analysis of meteorites, 3. C3 and C4 chondrites. *Earth and Planetary Science Letters*, 29(2), 283–290. [https://doi.org/10.1016/0012-821x\(76\)90132-1](https://doi.org/10.1016/0012-821x(76)90132-1)
- Ireland, M. J., & Kraus, A. L. (2008). The disk around CoKu tauri/4: Circumbinary, not transitional. *The Astrophysical Journal*, 678(1), L59–L62. <https://doi.org/10.1086/588216>
- Jiang, Z., Liu, Q., Dekkers, M. J., Zhao, X., Roberts, A. P., Yang, Z., et al. (2017). Remagnetization mechanisms in Triassic red beds from South China. *Earth and Planetary Science Letters*, 479, 219–230. <https://doi.org/10.1016/j.epsl.2017.09.019>
- Johnson, B. C., Walsh, K. J., Minton, D. A., Krot, A. N., & Levison, H. F. (2016). Timing of the formation and migration of giant planets as constrained by CB chondrites. *Science Advances*, 2(12), e1601658. <https://doi.org/10.1126/sciadv.1601658>
- Jull, A. J. T. (2006). Terrestrial ages of meteorites. In D. S. Lauretta, & H. Y. McSween (Eds.), *Meteorites and the early solar system II* (pp. 889–905). University of Arizona Press.
- Kirschvink, J. L. (1980). The least-squares line and plane and the analysis of paleomagnetic data: Examples from Siberia and Morocco. *Geophysical Journal of the Royal Astronomical Society*, 62(3), 699–718. <https://doi.org/10.1111/j.1365-246x.1980.tb02601.x>
- Kirschvink, J. L., Kopp, R. E., Raub, T. D., Baumgartner, C. T., & Holt, J. W. (2008). Rapid, precise, and high-sensitivity acquisition of paleomagnetic and rock-magnetic data: Development of a low-noise automatic sample changing system for superconducting rock magnetometers. *Geochimistry, Geophysics, Geosystems*, 9(5). <https://doi.org/10.1029/2007GC001856>
- Kita, N. T., & Ushikubo, T. (2011). Evolution of protoplanetary disk inferred from ^{26}Al chronology of individual chondrules. *Meteoritics & Planetary Sciences*, 47(7), 1108–1119. <https://doi.org/10.1111/j.1945-5100.2011.01264.x>
- Kletetschka, G., & Wiczorek, M. A. (2017). Fundamental relations of mineral specific magnetic carriers for paleointensity determination. *Physics of the Earth and Planetary Interiors*, 272, 44–49. <https://doi.org/10.1016/j.pepi.2017.09.008>
- Krot, A. N., Amelin, Y., Cassen, P., & Meibom, A. (2005). Young chondrules in CB chondrites from a giant impact in the early Solar System. *Nature*, 436(7053), 989–992. <https://doi.org/10.1038/nature03830>
- Krot, A. N., Hutcheon, I. D., Brearley, A. J., Pravdivtseva, O. V., Petaev, M. I., & Hohenberg, C. M. (2006). Timescales and settings for alteration of chondritic meteorites. In D. S. Lauretta, & H. Y. McSween (Eds.), *Meteorites and the early solar system II* (pp. 525–553). University of Arizona Press.
- Kruijer, T. S., Kleine, T., & Borg, L. E. (2020). The great isotopic dichotomy of the early Solar System. *Nature Astronomy*, 4(1), 32–40. <https://doi.org/10.1038/s41550-019-0959-9>
- Li, Y., Rubin, A. E., & Hsu, W. (2021). Formation of metallic-Cu-bearing mineral assemblages in type-3 ordinary and CO chondrites. *American Mineralogist*, 106(11), 1751–1767. <https://doi.org/10.2138/am-2021-7689>
- McClelland, E. (1996). Theory of CRM acquired by grain growth, and its implications for TRM discrimination and paleointensity determination in igneous rocks. *Geophysical Journal International*, 126(1), 271–280. <https://doi.org/10.1111/j.1365-246X.1996.tb05285.x>
- Mighani, S., Wang, H., Shuster, D. L., Borlina, C. S., Nichols, C. I. O., & Weiss, B. P. (2020). The end of the lunar dynamo. *Science Advances*, 6(1), eaax0883. <https://doi.org/10.1126/sciadv.aax0883>
- Morbidelli, A., Walsh, K. J., O'Brien, D. P., Minton, D. A., & Bottke, W. F. (2015). The dynamical evolution of the asteroid belt. *Asteroids, IV*, 493–507. https://doi.org/10.2458/azu_uapress_9780816532131-ch026
- Nagata, T., Funaki, M., & Kojima, H. (1991). Magnetic properties and natural remanent magnetization of carbonaceous chondrites containing pyrrhotite. *Proceedings of the NIPR Symposium on Antarctic Meteorites*, 4, 390–403.
- Nagy, L., Williams, W., Tauxe, L., Muxworthy, A. R., & Ferreira, I. (2019). Thermomagnetic recording fidelity of nanometer-sized iron and implications for planetary magnetism. *Proceedings of the National Academy of Sciences of the United States of America*, 116(6), 1984–1991. <https://doi.org/10.1073/pnas.1810797116>
- O'Brien, T., Tarduno, J. A., Anand, A., Smirnov, A. V., Blackman, E. G., Carroll-Nellenback, J., & Krot, A. N. (2020). Arrival and magnetization of carbonaceous chondrites in the asteroid belt before 4562 million years ago. *Communications Earth & Environment*, 1, 1–7. <https://doi.org/10.1038/s43247-020-00055-w>
- Oran, R., Weiss, B. P., & Cohen, O. (2018). Were chondrites magnetized by the early solar wind? *Earth and Planetary Science Letters*, 492, 222–231. <https://doi.org/10.1016/j.epsl.2018.02.013>
- Owen, J. E. (2016). The origin and evolution of transition discs: Successes, problems, and open questions. *PASA: Publications of the Astronomical Society of Australia*, 33, e005. <https://doi.org/10.1017/pasa.2016.2>
- Paterson, G. A., Tauxe, L., Biggin, A. J., Shaar, R., & Jonestrask, L. C. (2014). On improving the selection of Thellier-type paleointensity data. *Geochimistry, Geophysics, Geosystems*, 15(4), 1180–1192. <https://doi.org/10.1002/2013gc005135>
- Pravdivtseva, O., Meshik, A., & Hohenberg, C. M. (2013). The I-Xe record: Early onset of aqueous alteration in magnetites separated from CM and CV chondrites. *Lunar Planet Science Conference, XLIV*. abstract #3104.

- Scally, A., & Clarke, C. (2001). Destruction of protoplanetary discs in the orion nebula cluster. *Monthly Notices of the Royal Astronomical Society*, 325(2), 449–456. <https://doi.org/10.1046/j.1365-8711.2001.04274.x>
- Schrader, D. L., Davidson, J., McCoy, T. J., Zega, T. J., Russell, S. S., Domanik, K. J., & King, A. J. (2021). The Fe/S ratio of pyrrhotite group sulfides in chondrites: An indicator of oxidation and implications for return samples from asteroids Ryugu and Bennu. *Geochimica et Cosmochimica Acta*, 303, 66–91. <https://doi.org/10.1016/j.gca.2021.03.019>
- Scott, E. R. D., Keil, K., & Stöffler, D. (1992). Shock metamorphism of carbonaceous chondrites. *Geochimica et Cosmochimica Acta*, 56(12), 4281–4293. [https://doi.org/10.1016/0016-7037\(92\)90268-n](https://doi.org/10.1016/0016-7037(92)90268-n)
- Scott, E. R. D., & Krot, A. N. (2013). Chondrites and their components. In H. D. Holland, & K. K. Turekian (Eds.), *Treatise on geochemistry, planets, asteroids, comets, and the solar system* (pp. 66–137). Elsevier Science.
- Scott, E. R. D., Krot, A. N., & Sanders, I. S. (2018). Isotopic dichotomy among meteorites and its bearing on the protoplanetary disk. *The Astrophysical Journal*, 854(2), 164. <https://doi.org/10.3847/1538-4357/aaa5a5>
- Shadmehri, M., & Ghoreyshi, S. M. (2019). Time-dependent evolution of the protoplanetary discs with magnetic winds. *Monthly Notices of the Royal Astronomical Society*, 488(4), 4623–4637. <https://doi.org/10.1093/mnras/stz2025>
- Smith, R. J. (2009). Use and misuse of the reduced major axis for line-fitting. *American Journal of Physical Anthropology*, 140(3), 476–486. <https://doi.org/10.1002/ajpa.21090>
- Sridhar, S., Bryson, J. F. J., King, A. J., & Harrison, R. J. (2021). Constraints on the ice composition of carbonaceous chondrites from their magnetic mineralogy. *Earth and Planetary Science Letters*, 576, 117243. <https://doi.org/10.1016/j.epsl.2021.117243>
- Stephenson, A. (1983). Changes in the direction of the remanence of rocks produced by stationary alternating field demagnetization. *Geophysical Journal of the Royal Astronomical Society*, 73(1), 213–239. <https://doi.org/10.1111/j.1365-246x.1983.tb03815.x>
- Stephenson, A. (1993). Three-axis alternating field demagnetization of rocks and the identification of natural remanent magnetization, gyro-magnetic magnetization, and anisotropy. *Journal of Geophysical Research*, 98(B1), 373–381. <https://doi.org/10.1029/92jb01849>
- Sternberg, M. G., & Crowley, J. W. (2013). Thermal evolution of early solar system planetesimals and the possibility of sustained dynamos. *Physics of the Earth and Planetary Interiors*, 214, 53–73. <https://doi.org/10.1016/j.pepi.2012.10.006>
- Sutton, S., Alexander, C. M. O., Bryant, A., Lanzirotti, A., Newville, H., & Cloutis, E. A. (2017). The bulk valence state of Fe and the origin of iron in chondrites. *Geochimica et Cosmochimica Acta*, 211, 115–132. <https://doi.org/10.1016/j.gca.2017.05.021>
- Suzuki, T. K., Ogihara, M., Morbidelli, A., Crida, A., & Guillot, T. (2016). Evolution of protoplanetary discs with magnetically driven disc winds. *Astronomy & Astrophysics*, 596, A74. <https://doi.org/10.1051/0004-6361/201628955>
- Tauxe, L., & Staudigel, H. (2004). Strength of the geomagnetic field in the cretaceous normal superchron: New data from submarine basaltic glass of the troodos ophiolite. *Geochemistry, Geophysics, Geosystems*, 5(2). <https://doi.org/10.1029/2003GC000635>
- Tikoo, S. M., Weiss, B. P., Buz, J., Lima, E. A., Shea, E. K., Melo, G., & Grove, T. L. (2012). Magnetic fidelity of lunar samples and implications for an ancient core dynamo. *Earth and Planetary Science Letters*, 337–338, 93–103. <https://doi.org/10.1016/j.epsl.2012.05.024>
- Tikoo, S. M., Weiss, B. P., Cassata, W. S., Shuster, D. L., Gattacceca, J., Lima, E. A., et al. (2014). Decline of the lunar core dynamo. *Earth and Planetary Science Letters*, 404, 89–97. <https://doi.org/10.1016/j.epsl.2014.07.010>
- Tikoo, S. M., Weiss, B. P., Shuster, D. L., Suavet, C., Wang, H., & Grove, T. L. (2017). A two-billion-year history for the lunar dynamo. *Science Advances*, 3(8), e1700207. <https://doi.org/10.1126/sciadv.1700207>
- Torrano, Z. A., Schrader, D. L., Davidson, J., Greenwood, R. C., Dunlap, D. R., & Wadhwa, M. (2021). The relationship between CM and CO chondrites: Insights from combined analyses of titanium, chromium, and oxygen isotopes in CM, CO, and ungrouped chondrites. *Geochimica et Cosmochimica Acta*, 301, 70–90. <https://doi.org/10.1016/j.gca.2021.03.004>
- Wang, H., & Kent, D. V. (2021). Reset: A method to monitor thermoremanent alteration in the lillier-series paleointensity experiments. *Geophysical Research Letters*, 48(5), e2020GL091617. <https://doi.org/10.1029/2020GL091617>
- Wang, H., Weiss, B. P., Bai, X.-N., Downey, B. G., Wang, J., Wang, J., et al. (2017). Lifetime of the solar nebula constrained by meteorite paleomagnetism. *Science*, 355(6325), 623–627. <https://doi.org/10.1126/science.aaf5043>
- Weiss, B. P., Bai, X.-N., & Fu, R. R. (2021). History of the solar nebula from meteorite paleomagnetism. *Science Advances*, 7(1), eaba5967. <https://doi.org/10.1126/sciadv.aba5967>
- Weiss, B. P., & Bottke, W. F. (2021). What can meteorites tell us about the formation of Jupiter? *AGU Advances*, 2, e2020AV000376. <https://doi.org/10.1029/2020AV000376>
- Weiss, B. P., Gattacceca, J., Stanley, S., Rochette, P., & Christensen, U. R. (2010). Paleomagnetic records of meteorites and early planetesimal differentiation. *Space Science Reviews*, 152(1–4), 341–390. <https://doi.org/10.1007/s11214-009-9580-z>
- Weiss, B. P., & Tikoo, S. M. (2014). The lunar dynamo. *Science*, 346(6214). <https://doi.org/10.1126/science.1246753>
- Weiss, B. P., Wang, H., Sharp, T. G., Gattacceca, J., Shuster, D. L., Downey, B., et al. (2017). A nonmagnetic differentiated early planetary body. *Earth and Planetary Science Letters*, 468, 119–132. <https://doi.org/10.1016/j.epsl.2017.03.026>
- Yu, Y., Tauxe, L., & Genevey, A. (2004). Toward an optimal geomagnetic field intensity determination technique. *Geochemistry, Geophysics, Geosystems*, 5(2). <https://doi.org/10.1029/2003GC000630>
- Zhu, Z., Nelson, R. P., Hartmann, L., Espaillat, C., & Calvet, N. (2011). Transitional and pre-transitional disks: Gap opening by multiple planets? *The Astrophysical Journal*, 729(1), 47. <https://doi.org/10.1088/0004-637X/729/1/47>